

Copyright © 1994, by the author(s).  
All rights reserved.

Permission to make digital or hard copies of all or part of this work for personal or classroom use is granted without fee provided that copies are not made or distributed for profit or commercial advantage and that copies bear this notice and the full citation on the first page. To copy otherwise, to republish, to post on servers or to redistribute to lists, requires prior specific permission.

**GLOBAL MODEL OF Ar, O<sub>2</sub>, Cl<sub>2</sub> AND Ar/O<sub>2</sub>  
HIGH DENSITY PLASMA DISCHARGES**

by

C. Lee and M. A. Lieberman

Memorandum No. UCB/ERL M94/49

27 June 1994

(Revised 28 November 1994)

COVER PAGE

**GLOBAL MODEL OF Ar, O<sub>2</sub>, Cl<sub>2</sub> AND Ar/O<sub>2</sub>  
HIGH DENSITY PLASMA DISCHARGES**

by

C. Lee and M. A. Lieberman

Memorandum No. UCB/ERL M94/49

27 June 1994

(Revised 28 November 1994)

**ELECTRONICS RESEARCH LABORATORY**

College of Engineering  
University of California, Berkeley  
94720

**GLOBAL MODEL OF Ar, O<sub>2</sub>, Cl<sub>2</sub> AND Ar/O<sub>2</sub>  
HIGH DENSITY PLASMA DISCHARGES**

by

C. Lee and M. A. Lieberman

Memorandum No. UCB/ERL M94/49

27 June 1994

(Revised 28 November 1994)

**ELECTRONICS RESEARCH LABORATORY**

College of Engineering  
University of California, Berkeley  
94720

## **Global Model of Ar, O<sub>2</sub>, Cl<sub>2</sub> and Ar/O<sub>2</sub> High Density Plasma Discharges**

**C. Lee**

*Department of Chemical Engineering, University of California, Berkeley, California 94720*

**M. A. Lieberman**

*Department of Electrical Engineering and Computer Sciences, University of California, Berkeley, California, 94720*

We develop a global (volume averaged) model of high density plasma discharges in molecular gases. For a specified discharge length and diameter, absorbed power, pressure, and feed gas composition, as well as the appropriate reaction rate coefficients and surface recombination constants, we solve the energy and particle balance equations to determine all species densities and the electron temperature. We use an expression for charged particle diffusive loss that is valid for low and high pressures and for electropositive and electronegative plasmas. We apply the model to Ar, O<sub>2</sub>, Cl<sub>2</sub> and Ar/O<sub>2</sub> discharges and compare with available experimental data. In Ar, we find that the ion density increases monotonically with increasing pressure, while for O<sub>2</sub> and Cl<sub>2</sub>, the total positive ion density increases initially, then decreases as pressure is further increased. For a pure Cl<sub>2</sub> discharge, we find that surface recombination processes are important in affecting the degree of dissociation and the negative ion density of the system. For mixtures of Ar and O<sub>2</sub>, we find that at a fixed ratio of Ar to O<sub>2</sub> flowrates, the dominant ionic species changes from Ar<sup>+</sup> to O<sup>+</sup> as pressure is increased. When a small amount of Ar is added to a pure O<sub>2</sub> discharge, the overall positive ion density increases, whereas the ratio of negative ion to electron density decreases.

## I. INTRODUCTION

Molecular gases and their mixtures are used in the microelectronics industry for processing steps such as thin film etching and deposition. More specifically, electronegative gases such as chlorine and chlorine-containing mixtures are used for etching polysilicon, silicon oxide, and aluminum. The gas chemistry of these discharges, however, is poorly understood. Modelling of the plasma chemistry of electronegative discharges has been mainly in the intermediate pressure regime of several hundred mTorr to 1 Torr in parallel plate RF reactors.<sup>1-6</sup> Recently, Bassett and Economou<sup>7</sup> studied the effect of chlorine addition to an argon discharge; the model conditions, however, remained in the range of 0.3 - 1 Torr. Vender et al<sup>8</sup> have measured and modelled negative ion densities in an oxygen discharge, along with work done by Stoffels et al<sup>9</sup> to study the ion kinetics in discharges of Ar/CF<sub>4</sub> and Ar/CCl<sub>2</sub>F<sub>2</sub>. The pressure ranges in these studies were between 5 - 200 mTorr; however, the discharge used was a capacitively coupled RF plasma.

High density discharges such as radio frequency (RF) driven transformer-coupled-plasma (TCP) sources are becoming more preferable than conventional parallel plate reactors for ultra-large scale integrated circuit processing. These discharges typically operate at low pressures of 1 - 20 mTorr and high input powers of 1- 3 kW. The power absorption in a TCP source is typically inductive, as compared to the capacitive power absorption in an RF parallel plate reactor. Differences in the operating conditions between capacitively and inductively coupled sources can lead to drastically different behaviors in the plasma chemistry. For example, high density discharges can be highly dissociated, hence decreasing the negative ion concentration in the plasma by depleting the molecular source for negative ion formation. In this paper, we examine a volume-averaged (global) model of the plasma chemistry of some molecular gases and their mixtures, and compare this model to that of a pure argon discharge. A generalized power balance expression is developed that can be easily extended to include mixtures and polyatomic gases. The power balance includes energy loss channels for electron-neutral collisions such as rotational, vibrational, and electronic excitation, dissociation, ionization, dissociative attachment, and electron detachment. In addition, energy loss processes for heavy particle collisions such as asymmetric charge-exchange and ion-ion recombination are included. Particle balances are written for all species of interest. For the charged particles, the appropriate ambipolar diffusion rates in the presence of negative ions are used to determine the positive ion losses. The complete set of equations is solved self-consistently to obtain all species concentrations and the electron temperature.

## II. MODEL FORMULATION

## Assumptions

The cylindrical reactor geometry chosen was based on that of a commercially available TCP (transformer coupled plasma) reactor, with  $L = 7.5$  cm and  $R = 15.25$  cm (Fig. 1a). Assumptions of the model are listed below:

- 1). All densities  $n$  are assumed to be volume averaged; i.e.,

$$n = \frac{1}{\pi R^2 L} 2\pi \int_0^R r dr \int_0^L n(r, z) dz .$$

- 2). For an electropositive discharge, as shown in Fig. 1b, the positive ion densities are assumed to have a uniform profile throughout the discharge except near the wall, where the density is assumed to drop sharply to a sheath-edge density  $n_{iS}$ .
- 3). For an electronegative discharge, as shown in Fig. 1c, the electron density  $n_e$  is assumed to be uniform throughout the discharge except near the sheath edge. The negative ion density  $n_-$  is assumed to be parabolic, dropping to zero at the sheath edge, the positive ion density is  $n_i = n_e + n_-$ , with  $n_i = n_e = n_{iS}$  at the sheath edge. An appropriate interpolation between electropositive and electronegative profiles is used, as described in the Appendix. The relationship between the bulk positive ion density  $n_i$  and the edge density  $n_{iS}$  is discussed later in this section and in the Appendix.
- 4). We neglect the energy losses for processes in which one ion is dissociated to form another and we neglect energy losses due to collisions of electrons with positive or negative ions, because in the regime of interest, the charged particle densities are small compared to the neutral densities.
- 5). We neglect electron dissociation of molecular ions in the particle balance because in high density sources, the molecular ion density is small.<sup>10</sup>
- 6). We assume only one type of negative ion is generated.
- 7). The factors  $h_L$  and  $h_R$  are assumed to be independent of the type of ions; i.e., the ion-neutral mean free path  $\lambda$  is identical for all species in the discharge.
- 8). The ion temperature  $T_i$  is assumed to be 0.5 eV for pressures less than 1 mTorr; for higher pressures,  $T_i - T_0$  is allowed to decrease at a rate proportional to  $1/p$ , ultimately reaching the thermal temperature of  $T_0 = 600$  K. The neutral temperature was assumed to be 600 K.

## Generalized Power Balance

Two main sets of equations are used in the global model: power balance and particle balance for all species of interest. For a monatomic gas, the equations are straightforward, as discussed by Lieberman and Gottscho<sup>11</sup>. For an argon discharge, ignoring the presence of metastables, the electron temperature ( $T_e$ , in units of eV) is simply a function of the pressure and geometry of the system, the plasma density is proportional to the input power, and the collisional energy loss per electron-ion pair created ( $\epsilon_L$ , in units of eV) is a function of  $T_e$  only. For molecular gases, the situation is more complicated. As we will see, the plasma composition, i.e., ion and neutral densities, plays an important role in determining the electron temperature and  $\epsilon_L$ .

The total power balance has the general form of

$$P_{abs} = P_{ev} + P_{iw} + P_{ew} , \quad (1)$$

where  $P_{abs}$  is the power absorbed by the system,  $P_{ev}$  is the electron energy loss due to all electron-neutral collision processes in the volume,  $P_{iw}$  is the ion energy loss to the walls, and  $P_{ew}$  is the electron energy loss to the walls. For an atomic gas, the energy loss  $\epsilon_L$  per electron-ion pair created due to all electron neutral collision processes can be expressed as

$$v_{iz} \epsilon_L = v_{iz} \epsilon_{iz} + \sum_{k=1}^{N_{exc}} v_{exc,k} \epsilon_{exc,k} + v_{elas} \frac{3T_e}{2} \frac{2m}{M}, \quad (2)$$

where  $v = \langle \sigma v \rangle n_n$  is the appropriate collision frequency,  $\langle \sigma v \rangle$  is the rate coefficient,  $n_n$  is the neutral density, and  $N_{exc}$  is the number of excitation energy loss channels. The first term on the right hand side of Eq. (2) is the energy loss due to the ionization of neutral atoms with an ionization potential of  $\epsilon_{iz}$  (in units of eV), the second term represents the total energy loss due to excitation of neutral atoms to various excited states with threshold energies  $\epsilon_{exc}$ , and the last term is the energy loss due to electron-neutral elastic scattering. If we divide Eq. (2) by  $v_{iz}$ , we obtain

$$\epsilon_L = \epsilon_{iz} + \sum_{k=1}^{N_{exc}} \frac{v_{exc,k}}{v_{iz}} \epsilon_{exc,k} + \frac{v_{elas}}{v_{iz}} \left( \frac{3mT_e}{M} \right) . \quad (3)$$

Since the ratios of collision frequencies are equal to the corresponding ratios of rate constants independent of the atomic gas density,  $\epsilon_L$  is a function of  $T_e$  only.

Ion energy is lost to the wall at a characteristic velocity which is the Bohm velocity  $u_B =$

$(eT_e/M)^{1/2}$ , with  $e = 1.6 \times 10^{-19} \text{C}$ ,

$$P_{iw} = en_s u_B A \epsilon_{iw} \quad , \quad (4)$$

where  $n_s$  is the ion sheath edge density,  $A$  is the surface area of the chamber walls, and  $\epsilon_{iw}$  is the ion kinetic energy lost per ion lost to the wall, which is typically between 5-8  $T_e$  for high density sources; the electron energy lost to the wall has the form

$$P_{ew} = en_{es} u_B A \epsilon_{ew} \quad , \quad (5)$$

where  $\epsilon_{ew} = 2T_e$  is the electron kinetic energy lost per electron lost to the walls.

For molecular gases, several complications can arise: i) generation of multiple positive ions are possible; ii) fragmentation of the neutral molecule can provide multiple neutral molecule sources for generation of ions; iii) generation of negative ions is possible; and iv) additional energy loss channels such as dissociation, and particle loss channels such as volume positive-negative ion recombination, need to be included. These factors require modification of Eqs. (1) and (2). We rewrite Eq. (1) as

$$P_{abs} = \sum_{i=1}^r P_{iw,i} + P_{ev} + P_{ew} \quad , \quad (6)$$

where  $r$  is the number of positive ion species generated in the system, i.e., for  $\text{O}_2$ ,  $r = 2$ , for generation of both  $\text{O}_2^+$  and  $\text{O}^+$ . Equation (2) is modified to be

$$v_{iz,i} \epsilon_{L,i} = \sum_{j=1}^{N_{s,i}} \left( v_{iz,ij} \epsilon_{iz,ij} + \sum_{k=1}^{N_{exc,j}} v_{exc,kj} \epsilon_{exc,kj} + v_{elas,j} \frac{2m}{M_j} \frac{3T_e}{2} \right) \quad , \quad (7)$$

where  $N_{s,i}$  is the number of neutral species that generates the  $i$ th ion. For  $\text{Ar}^+$ ,  $N_{s,i} = 2$  (Ar and  $\text{Ar}^*$ ); for  $\text{O}^+$ ,  $N_{s,i} = 2$  (O and  $\text{O}^*$ ); for  $\text{O}_2^+$ ,  $N_{s,i} = 1$  ( $\text{O}_2$ ); for  $\text{Cl}^+$ ,  $N_{s,i} = 1$  (Cl); and for  $\text{Cl}_2^+$ ,  $N_{s,i} = 1$  ( $\text{Cl}_2$ ). We have not included  $\text{O}_2^*$  in  $N_{s,i}$  because a previous study showed that the  $\text{O}_2^*$  concentration is much lower than that of the atomic species.<sup>10</sup> In Eq. (7),  $v_{iz,ij}$  is the ionization frequency for production of the  $i$ th ion from neutral species  $j$ ,  $v_{iz,i}$  is the total ionization frequency for production of the  $i$ th ion,  $\epsilon_{iz,ij}$  is the threshold ionization energy for production of the  $i$ th ion from neutral species  $j$ ,  $\epsilon_{exc,kj}$  is the threshold excitation energy for the  $k$ th level of the  $j$ th neutral, and  $\epsilon_{L,i}$  is the total collisional energy loss per electron-ion pair created for the  $i$ th ion. The sum over  $k$  includes all inelastic electron-neutral collisional processes that do not produce positive ions; e.g., rotational, vibrational and electronic excitation, dissociation, attachment and detachment.

Dividing Eq. (7) by  $v_{iz,i}$ ,  $\epsilon_{L,i}$  can be expressed as

$$\epsilon_{L,i} = \frac{1}{v_{iz,i}} \sum_{j=1}^{N_{si}} \left( v_{iz,ij} \epsilon_{iz,ij} + \sum_{k=1}^{N_{exc,j}} v_{exc,kj} \epsilon_{exc,kj} + \frac{v_{elas,j} 3mT_e}{M_j} \right). \quad (8)$$

An average energy loss factor  $\epsilon_L$  can also be defined for complicated gases and mixtures:

$$\epsilon_L \sum_{i=1}^r v_{iz,i} = \sum_{i=1}^r \epsilon_{L,i} v_{iz,i}$$

From Eq. (8), we can see that once there are multiple sources for generating the same ion,  $\epsilon_{L,i}$  is no longer a function of  $T_e$  only, but is also a function of the neutral composition in the plasma. The right hand side of Eq. (8) includes only the possible channels for electron energy loss; electrons can also gain energy through collisions. For example, in the case of argon, metastables ( $\text{Ar}^*$ ) are known to be destroyed by superelastic quenching<sup>12-15</sup>,



In this situation, an extra term is added to the RHS of Eq. (8),

$$\epsilon_{\text{gain}} = \left( -\frac{1}{v_{iz,i}} \right) v_q \epsilon_q,$$

where  $v_q$  is the de-excitation frequency and  $\epsilon_q$  is the energy gained per collision.

Using the continuity equation for the  $i$ th positive ion, including volume losses due to positive-negative ion recombination and asymmetric charge exchange (for the case of mixtures), we have

$$V n_e v_{iz,i} = A n_{is} u_{B,i} + V k_{rec,i} n_i n_- + V \sum_{j=1}^{N_s} k_{cx,ij} n_i n_j, \quad (9)$$

where  $V$  is the reactor volume,  $k_{rec,i}$  is the recombination rate coefficient,  $k_{cx,ij}$  is the charge exchange rate coefficient for asymmetric collisions between the  $i$ th ion and the  $j$ th neutral, and  $n_-$  is the negative ion density. The last term on the RHS of Eq. (9) is the loss of the  $i$ th ion through collisions with the  $j$ th neutral to generate another ionic species, hence, for the ion that is generated from the  $j$ th neutral, the asymmetric charge exchange reaction will appear as a generation term in the particle balance equation rather than a loss term. The densities at the sheath edge are related

by the quasineutrality condition,

$$n_{es} = \sum_{i=1}^r n_{is} , \quad (10)$$

and the total power lost in the volume is

$$P_{ev} = en_e V \sum_{i=1}^r v_{iz,i} \epsilon_{L,i} \quad (11)$$

Substituting Eq. (10) into Eq. (5), and Eq. (9) into Eq. (11), the total power balance of Eq. (6) becomes

$$P_{abs} = \sum_{i=1}^r en_i \left( A_{eff} \epsilon_{T,i} u_{B,i} + k_{rec,i} n_- \epsilon_{L,i} V + \sum_{j=1}^{N_s} k_{cx,ij} n_j \epsilon_{L,i} V \right), \quad (12)$$

in which  $A_{eff}$  is the effective surface area for ion loss<sup>11</sup>,

$$A_{eff} = \frac{n_{is}}{n_i} \Big|_{axial} 2\pi R^2 + \frac{n_{is}}{n_i} \Big|_{radial} 2\pi RL ,$$

and

$$\epsilon_{T,i} = \epsilon_{L,i} + \epsilon_{iw} + \epsilon_{ew} .$$

The ratio of sheath edge density  $n_{is}$  to the bulk average density  $n_i$  is derived in the Appendix and is found to be

$$h_L = \frac{n_{is}}{n_i} \Big|_{axial} = \frac{1 + \frac{3\alpha_{avg}}{\gamma}}{1 + \alpha_{avg}} \frac{0.86}{\left( 3 + \frac{L}{2\lambda} + \left( \frac{0.86Lu_B}{\pi D_a} \right)^2 \right)^{1/2}} , \quad (13)$$

at the axial sheath edge ( $z = 0$  and  $z = L$ ) and

$$h_R = \frac{n_{is}}{n_i} \Big|_{radial} = \frac{1 + \frac{3\alpha_{avg}}{\gamma}}{1 + \alpha_{avg}} \frac{0.8}{\left( 4 + \frac{R}{\lambda} + \left( \frac{0.8Ru_B}{2.405 (J_1(2.405) D_a)} \right)^2 \right)^{1/2}} , \quad (14)$$

at the radial sheath edge ( $r = R$ ). Here  $\alpha_{avg} = n_-/n_e$  is the ratio of negative ion to electron density.

$\gamma = T_e/T_i$ ,  $\lambda$  is the ion-neutral mean free path,  $D_a$  is the ambipolar diffusion coefficient, and  $J_1$  is the Bessel function of the first order. The assumptions stated earlier about  $h_L$  and  $h_R$  mean that the ion-neutral momentum transfer cross sections are independent of the type of ion or neutral present in the plasma. For the systems we are interested in studying, this assumption is reasonable because the difference in atomic sizes for the neutrals is at the most a factor of two, i.e.,  $O_2$  versus  $O$ , or  $Cl$  vs  $Cl_2$ , leading to approximately the same factor of difference in the ion-neutral collision cross sections. Furthermore, since at the low pressures of interest we are taking the square root of  $\lambda$  in Eqs. (13) and (14), the error introduced by small differences in  $\lambda$  is small. The terms in Eqs. (13) and (14) involving the ambipolar diffusion coefficient  $D_a \sim eT_e/M_i v_i$ , with  $v_i = v_{thi}/\lambda$  and  $v_{thi}$  the ion thermal velocity, are important only at the highest pressures of interest. In calculating  $v_{thi}$ , the assumption of ion temperature  $T_i$  being 0.5 eV is valid for pressures less than 1 mTorr<sup>16,17</sup>; for higher pressures,  $T_i - T_o$  is allowed to decrease at a rate proportional to  $1/p$ , ultimately reaching the thermal temperature of  $T_o = 0.052$  eV.

### Discharges of Argon, Oxygen and Chlorine

The generalized electron power balance obtained in Eq. (12) enables us to study complicated gases and mixtures. We have applied the formulation to systems of atomic and molecular gases. The reaction sets used for Ar,  $O_2$ , and  $Cl_2$  and the excitation processes are listed in Tables 1- 5. Excitation processes for  $O_2$  can be found in a previous publication.<sup>10</sup> Types of electron-neutral reactions included are ionization, dissociation, excitation, dissociative excitation, dissociative attachment, and electron detachment. Dissociative ionization of molecular gas is not included for two reasons: 1). the threshold for this process is higher, and hence the reaction probability is low; 2) the density of molecular species is low due to the high dissociation rate, hence decreasing the overall rate of reaction. We have verified this by running the simulation with and without the dissociative ionization process, and found no significant difference in the results. Three-body recombination reactions are not included since at the pressure range of interest, i.e., less than 100 mTorr, the rate coefficients are orders of magnitude smaller compare to other processes. Ion-ion and neutral-neutral interactions are also included through the processes of positive-negative ion recombination and metastable quenching. Two-step ionization, i.e., excitation from the ground to a metastable state, followed by ionization from the metastable state, are included for Ar and  $O_2$ . We did not include metastables for the chlorine discharge, since metastables were found to be unimportant in contributing to the total positive ion density in  $O_2$  discharges due to their low concentration<sup>10</sup>, and the threshold energy (10 eV) required for the generation of  $Cl^*$  is much larger than that of  $O^*$  (2 eV). Chlorine metastables, presumably will have the same generation and loss mechanisms as that of  $O^*$ , hence, we concluded that  $Cl^*$  is unimportant. For argon, the largest loss rate of  $Ar^*$  was through superelastic quenching by cold electrons. Unlike oxygen, quenching of  $Ar^*$  by ground state Ar is not an efficient process due to the lack of vibrational and rotational energy levels in the atomic gas<sup>12-14</sup>. Besides volume quenching, we have also included wall quenching, in

which metastable species are de-excited upon striking the chamber walls, and the ground state species are returned to the reactor. This process is controlled by diffusion; hence the loss rate to the wall is largest at low pressure. The diffusional losses are represented in Tables 1-5 by  $k \sim D_{eff}/\Lambda^2$ , where  $D_{eff}$  is the effective diffusion coefficient of the neutral species of interest<sup>11</sup>, which has the expression

$$D_{eff} = \frac{1}{\left(\frac{1}{D_{AA^*}} + \frac{1}{D_{KN}}\right)},$$

where  $D_{AA^*}$  is the diffusion coefficient estimated using the Chapman-Enskog equation for gas diffusivity<sup>18</sup>, and  $D_{KN}$  is the Knudsen free-diffusion coefficient equal to  $v_{th}\Lambda/3$ ,  $\Lambda$  is the effective diffusion length given by

$$\frac{1}{\Lambda^2} = \left(\frac{\pi}{L}\right)^2 + \left(\frac{2.405}{R}\right)^2,$$

and  $v_{th} = (kT_o/M)^{1/2}$  is the neutral thermal velocity. The types of reactions used for  $\text{Cl}_2$  are identical to those of  $\text{O}_2$ , with the exclusion of metastables. The difference in the chemical nature of chlorine and oxygen, however, can lead to different results. For example, the bond strengths of  $\text{Cl}_2$  and  $\text{O}_2$  are 2.5 eV and 5.5 eV, respectively. The weaker chlorine bond generates more Cl under the same process conditions, therefore decreasing the concentration of negative ions in the discharge through depletion of the  $\text{Cl}_2$  source density for  $\text{Cl}^-$  production by electron attachment. The more electronegative nature of chlorine, however, tends to increase the  $\text{Cl}^-$  density because of a larger attachment rate coefficient to  $\text{Cl}_2$ . We will see the influence of these competing effects in the Results and Discussion Section.

The continuity equations for the neutrals is written based on the mass conservation principle of generation rate = loss rate. Details of the individual terms included for each type of mechanism can be found in reference 10.

## Mixtures of Argon and Oxygen

The chemistry of the discharge is complicated when mixtures are considered. Most processing discharges use mixtures of two or more gases in order to achieve the desired etch profile, selectivity, and etch rate. We choose to study a mixture of argon and oxygen. The chemistry of this system allows us to capture some effects of gas mixtures on the discharge parameters. The reactions that describe the interaction between argon and oxygen are listed in Table 6. The presence of  $\text{Ar}^+$  can act as an additional loss channel for negative ions through ion-ion recombination, and  $\text{Ar}^*$  can be de-excited by both neutral  $\text{O}_2$  and O. We have not considered Penning ionization, i.e., ionization of neutral species by metastables, since neither  $\text{Ar}^*$  nor  $\text{O}^*$  has enough energy to

overcome the ionization thresholds of O<sub>2</sub>, O, and Ar. We have, however, included dissociation of O<sub>2</sub> by metastable argon. Nonresonant exothermic charge exchange was also included, in which Ar<sup>+</sup> is charge exchanged with O<sub>2</sub> and O; the reverse reactions were not considered because the energies carried by O<sub>2</sub><sup>+</sup> and O<sup>+</sup>, 12.6 and 13.6 eV, respectively, are not sufficient to ionize Ar, whose ionization potential is 15.6 eV.

### III. RESULTS AND DISCUSSION

Equation (12) for power balance is solved simultaneously with particle balances for each species, and charge neutrality is used to obtain the electron density. The pressure of the system is calculated based on neutrals only, with  $p = \sum n_j kT$ , where  $n_j$  is the  $j$ th neutral species and  $T$  is the neutral temperature. Input parameters for the model are power, inlet pressure, which is determined from density of the feed gas Cl<sub>2</sub>; flowrate, composition of the neutral feed gas, and surface recombination coefficient  $\gamma_{rec}$  for O or Cl. The inlet pressure is defined as the pressure when the discharge is off, and hence is based on the density of the neutral feed gas only. Unless otherwise indicated, the results presented in this paper are at a fixed absorbed power of 1000 W and total flowrate of 35 SCCM. Pressure, feed gas composition, and  $\gamma_{rec}$  are varied, and their effects on fractional dissociation, electronegativity, and plasma composition are studied. In this section, we first describe the differences between atomic and molecular gases. Next we compare the two different molecular gases, and finally, we present results for a mixture of atomic and molecular gases.

#### Atomic and Molecular Gases

A major difference between atomic and molecular gases is the availability of energy loss channels. Electrons, upon colliding with neutral atoms/molecules, can lose energy and excite the heavy particle into an electronically or vibrationally-rotationally excited state. For an atomic gas, there are no vibrational or rotational states available. Hence the collisional energy lost per electron-ion pair created  $\epsilon_L$  is much less for a monatomic gas than for a diatomic gas, especially at low electron temperatures, where  $\epsilon_L$  is dominated by excitation losses (See Fig. 2).

Figure 3 shows the electron temperature dependence on pressure for pure Ar, O<sub>2</sub>, and Cl<sub>2</sub> discharges. The trends are similar, with  $T_e$  decreasing with increase pressure. The difference in the values of  $T_e$  demonstrates that the electron temperature is a function of the plasma composition. Under identical operating conditions, we see that  $T_e$  can differ by up to a factor of two or more, especially in the lower pressure range. The difference is due to the fact that  $T_e$  is determined from the particle balances<sup>11</sup>, and because we have included balances for both neutral and charged species,  $T_e$  is determined by the dominant ion/neutral component of the discharge. Depending upon the species present in the greatest amount,  $T_e$  will vary accordingly. The total positive ion density

for the three systems is presented in Fig. 4. An argon discharge consistently has the highest density for the entire pressure range studied. The molecular gases are at lower densities, with oxygen having the lowest overall  $n_+$ . The differences in the ion densities are due to the factors of  $\epsilon_L$  and  $A_{eff}$  in Eqs. (8) and (12). From Eq. (8), one can see that the electron energy loss is directly proportional to the number of available energy loss channels of the neutral species; hence,  $\epsilon_L$  for argon is much less than  $\epsilon_L$  for oxygen and chlorine, since there are fewer energy loss channels for the atomic gas. The effective loss area  $A_{eff}$  is a decreasing function of pressure because the ions are more confined at higher pressures. The energy loss factor  $\epsilon_L$ , on the other hand, increases with increasing  $p$ . Comparing the effects of  $\epsilon_L$  and  $A_{eff}$  in Eq. (12), we can see that as the pressure increases, the two factors vary in opposite directions. Whichever factor dominates will determine the behavior of the total positive ion density with pressure. From Fig. 4, one can conclude that at a fixed power, for Ar and  $\text{Cl}_2$ ,  $A_{eff}$  decreases faster than the increase in  $\epsilon_L$  as pressure increases, with the overall result that the ion density increases; for oxygen, however,  $n_+$  increase initially but decreases at higher pressures, which points to the dominance of  $\epsilon_L$  over  $A_{eff}$ .

### Oxygen and Chlorine Discharges

For molecular gases, surface recombination processes can be important, especially if the atom of interest has a high surface recombination coefficient<sup>19</sup>, as is believed to be the case of Cl. This reaction is the recombination of a gaseous atom with an adsorbed atom on the reactor wall, using the wall surface as a third body:



This provides an additional source for  $\text{Cl}_2$ , which enhances the electronegativity of the plasma. The  $\text{Cl}_2$  bond is weak, however, and the molecule can be dissociated, regenerating Cl and decreasing the negative ion concentration. These two competing effects strongly depend on the recombination coefficient  $\gamma_{rec}$ , as shown in Fig. 5. The ratio of  $n_-/n_e$  is plotted against  $\gamma_{rec}$  with pressure as a parameter for discharges of pure  $\text{O}_2$  and  $\text{Cl}_2$ . From Fig. 5a, we can see that the recombination coefficient does not have a major effect on the electronegativity of  $\text{O}_2$ ;  $n_-/n_e$  approaches unity at  $\gamma_{rec} = 0.4$  and a pressure of 100 mTorr. Note that this value of  $\gamma_{rec}$  suggests that four out of every ten oxygen atoms that strike the wall will recombine to form  $\text{O}_2$ . This is unlikely, because the surface recombination coefficient for oxygen on a clean surface is reported to be  $\sim 10^{-4}$ <sup>(20)</sup>. For a surface that is passivated with oxygen, the recombination coefficient is even lower due to the low physisorption surface coverage. For  $\text{Cl}_2$ , however, the situation is different. Chlorine is believed to have a high  $\gamma_{rec}$ , which has made it difficult for researchers to measure the Cl atom concentration in the afterglows of discharges<sup>21</sup>. Values of  $\gamma_{rec}$  reported in literature have been as high as 0.15<sup>19</sup>. Furthermore, chlorine is more electronegative than oxygen, and therefore, has a greater tendency to form negative ions due to the higher reaction probability or attachment

rate. From Fig. 5b, we see that the negative ion density exceeds the electron density at  $\gamma_{rec} = 0.08$  at a pressure of 100 mTorr. Interpolating between the 10 and 100 mTorr curves at  $\gamma_{rec} = 0.1$ , it is not difficult to see that negative ions can become important in the operating range of high density sources (1 - 20 mTorr). The difference in  $n_-/n_e$  for  $O_2$  and  $Cl_2$  is consistent with the chemical nature of the two gases, with chlorine being a more electronegative gas and  $Cl^-$  having a higher electron affinity than  $O^-$ , 3.62 vs 1.45 eV, respectively.

The effect of  $\gamma_{rec}$  on the total positive ion density,  $n_+$ , is presented in Fig. 6. Figure 6a shows that for an oxygen discharge, surface recombination has little effect on the total positive ion density. For the range of  $\gamma_{rec}$  investigated, the variation of  $n_+$  does not differ much compare to the  $\gamma_{rec} = 0$  case (see Fig. 4); for chlorine, however, Fig. 6b shows that surface recombination decreases  $n_+$  as  $\gamma_{rec}$  becomes greater than 0.05 in the high pressure regime. In this situation,  $Cl^+$  is no longer the dominant positive ion, and the densities of the two types of positive ions,  $Cl^+$  and  $Cl_2^+$ , are comparable in magnitude. The decrease in  $n_+$  is due to the increase in the energy loss factor  $\epsilon_L$ . Recall from Section II that the ion density is strongly affected by the collisional energy loss per electron-ion pair created, and since  $\epsilon_L$  for  $Cl_2$  much exceeds  $\epsilon_L$  for  $Cl$ , the total ion density drops as a result. The electron temperature,  $T_e$ , is also affected by  $\gamma_{rec}$  through the enhancement in electronegativity. The results show that at high pressures,  $T_e(\gamma_{rec}=0.1) > T_e(\gamma_{rec}=0)$  for both  $O_2$  and  $Cl_2$  due to the increase in the negative ion density. As  $n_-$  increases,  $n_e$  drops, hence the electron temperature must rise to sustain the required ionization rate<sup>10</sup>.

An additional variable that is of concern for high density discharges is the fractional dissociation of the neutral feed gas, which is defined as the ratio of the density of the atomic neutral, O or Cl, to the total neutral density. A high degree of dissociation will result in a high concentration of reactive free radicals which can directly influence process output parameters such as the etch rate. Figs. 7a and 7b show the effect of  $\gamma_{rec}$  on discharges of  $O_2$  and  $Cl_2$  for pressures of 1, 10, and 100 mTorr. For a large  $\gamma_{rec}$ , the fractional dissociation decreases as expected, since neutral atoms are depleted through wall recombination to generate neutral molecules. For the case of  $\gamma_{rec} = 0.1$ ,  $Cl_2$  is ~ 80% dissociated, whereas  $O_2$  is ~ 50% dissociated; the difference in fractional dissociation is partly due to the difference in bond strengths of each molecule, which is directly related to the collision cross section of the dissociation process; and the difference in electron temperatures. The double bond in the oxygen molecule makes it more difficult to dissociate  $O_2$  than  $Cl_2$ , which has a single bond. The bond energies are 5.5 vs. 2.5 eV, respectively; hence, under identical operating conditions, the fractional dissociation of  $O_2$  is lower than that of  $Cl_2$ . Note that the dependence of fractional dissociation on  $\gamma_{rec}$  is highly nonlinear. No significant changes in fractional dissociation are observed until  $\gamma_{rec} > 0.02$ .

## Comparison with Experimental Data

Model results for both Ar and  $Cl_2$  are compared with available experimental data. Oxygen

result comparisons were discussed in a previous publication<sup>10</sup> and are not included here. Figures 8 and 9 are comparisons of the total positive ion density versus pressure for Ar and Cl<sub>2</sub>, respectively. In both figures, the symbols are the experimental data, and the curves are the model results. In Fig. 8, Ra et al<sup>22</sup> (◆ symbol) gave values of ion current density in a TCP system rather than ion density, hence, we calculated  $J_{\text{ion}}$  using the expression  $J_{\text{ion}} = en_+u_B$ . Data from Mahoney et al<sup>23</sup> (■) were also obtained in a TCP system, whereas Oomori et al<sup>24</sup> (●) took measurements in an extended ECR source. For all three cases, the experimental data shows that the Ar<sup>+</sup> density increases monotonically with increasing pressure, which agrees qualitatively with values predicted by the model.

For a pure chlorine discharge, ion densities were measured by Ra et al and Oomori et al. The results are presented in Fig. 9 (■ - Ra et al; ● - Oomori et al). Both sets of experimental results show that the total positive ion density decreases slightly as the pressure is increased. The model predictions for  $J_{\text{ion}}$  show that the effect of  $\gamma_{\text{rec}}$  is small, and only small percentage differences were observed in the low pressure range of 0.2 - 5 mTorr. On the other hand, the model predictions for the ion density in the Oomori system show a significant dependence on  $\gamma_{\text{rec}}$ . For  $\gamma_{\text{rec}} = 0$ ,  $n_+$  steadily increases with increasing  $p$ , but with  $\gamma_{\text{rec}} = 0.1$ ,  $n_+$  increases initially and then decreases at higher pressures, which follows the experimental trend. The difference between the two sets of experimental data is due to the difference in the operating conditions and the geometry of the systems. In the ECR system, the volume is much larger and the flowrate is low (10 SCCM), hence the residence time is long. In the TCP, however, the volume is 13 times smaller, and there is a higher flowrate of 80 SCCM. This difference in residence times leads to significantly different ion compositions for the two systems, and hence a significantly different sensitivity to surface recombination processes. This change in the trend of  $n_+/J_{\text{ion}}$  vs  $p$  shows the importance of reactor geometry, operating conditions, and the strong coupling to surface reactions, which can affect the overall positive ion density.

## Mixtures of Argon and Oxygen

When argon is added to an oxygen discharge, the discharge becomes complicated. There are three types of positive ions, O<sub>2</sub><sup>+</sup>, O<sup>+</sup>, Ar<sup>+</sup>, and five different neutrals, O<sub>2</sub>, O, O<sup>\*</sup>, Ar, Ar<sup>\*</sup>, in addition to negative (O<sup>-</sup>) ions and electrons. The interactions between these species are listed in Table 6. The total flowrate into the system is held fixed at 35 SCCM, and the composition of the feed gas is varied to achieve a desired argon to oxygen ratio. The fraction of Ar ( $f_{\text{Ar}}$ ) used in Figs.10 and 11 is defined as the ratio of Ar flowrate to the total neutral flowrate. The pressure is varied from 1 - 50 mTorr. The fraction of ions that are Ar<sup>+</sup> is plotted in Fig.10 as a function of  $f_{\text{Ar}}$ . At a fixed feed gas composition, for example,  $f_{\text{Ar}} = 0.5$ , the fraction of Ar<sup>+</sup> decreases with increasing pressure. At 1 mTorr, Ar<sup>+</sup> makes up more than 50% of the total positive ion density, whereas at 50 mTorr, less than 30% of the positive ions are Ar<sup>+</sup>. This dependence on pressure can

be explained through the difference in the ionization rate coefficients for  $O^+$  and  $Ar^+$ . At low pressures,  $T_e$  is high (see Fig. 3), and the ionization of argon is favored since the ionization rate coefficient of Ar is larger than that of O for  $T_e > 2.5$  eV. At higher pressures,  $T_e$  is lower, and the generation of  $O^+$  is favored; in addition, asymmetric charge exchange between  $Ar^+/O$  and  $Ar^+/O_2$  also destroys argon ions, which further decreases the  $Ar^+$  density at high pressures. We did not include  $O_2^+$  in this comparison because the  $O_2^+$  density is much lower than that of  $O^+$ .

The effect of argon addition on the concentration of O atoms has also been investigated. The fraction of O atoms plotted in Fig. 11 is defined as the ratio of the O atom density to the total neutral density. The results show that the fraction is nearly independent of pressure, since both the O atom density ( $[O]$ ) and the total neutral density are nearly linearly dependent on pressure. The enhancement in  $[O]$  due to argon addition over that due to the dilution of the feed gas can be attributed to the changes in the electron temperature, which in turn affect the generation and loss rates associated with the oxygen atom.

The total positive ion density is also enhanced by the addition of argon. At low flows of argon into the system, the behavior of  $n_+$  with pressure follows the trends of an oxygen discharge, (see Fig. 4), where  $n_+$  peaks at approximately 10 mTorr, and decreases at higher pressures. At higher flowrates of argon, i.e.,  $f_{Ar} > 0.8$ ,  $n_+$  follows the trends of an argon discharge, where the ion density increases monotonically with increasing pressure. Another parameter of interest is the electronegativity of the discharge. The ratio of  $n/n_e$  was observed to decrease with addition of argon, since the source for negative ion generation ( $O_2^-$ ) is reduced, and the presence of  $Ar^+$  provides an additional loss mechanism for negative ions through ion-ion recombination.

#### IV. CONCLUSIONS

We have developed a generalized power balance equation for high density plasma discharges that can be easily extended to include gas mixtures and polyatomic gases. The equation was used to study discharges of  $Cl_2$ ,  $O_2$ , and  $Ar/O_2$  mixtures. We found that for molecular gases, the electron temperature  $T_e$  is no longer a function of pressure and the reactor geometry, but also strongly depends on the plasma composition. The difference in the energy loss channels for each feed gas leads to differences in plasma variables such as ion density, electron temperature, and plasma composition.

We studied the plasma chemistry of molecular gases and their mixtures in a high density discharge. Fractional dissociations of  $Cl_2$  and  $O_2$  under normal operating conditions of TCP reactors were shown to be essentially unity when surface recombination processes were not included. When surface reactions were added to the model, we found that the chlorine discharge was more sensitive to surface recombination rate than oxygen. The surface recombination coefficient for chlorine can be as high as 0.15; this high probability of surface recombination can increase the

electronegativity of the discharge by increasing the molecular gas concentration, and hence decreasing the fractional dissociation. For an oxygen discharge, the situation is different because the surface recombination rates are slow. In addition, the attachment coefficient for the formation of  $O^-$  is smaller than for  $Cl^-$ , hence, the electronegativity in an  $O_2$  discharge is lower than that of a  $Cl_2$  discharge under the same operating conditions.

For  $Ar/O_2$  mixtures, we found that at low pressures, the dominant ion in the argon-oxygen mixture is  $Ar^+$ ; at higher pressures, however, the dominant ionic species switches to  $O^+$ . The addition of argon changes the electron temperature of the system, which directly affects the rate coefficients. Since the rate coefficients are strong functions of  $T_e$ , we see an increase in the concentration of O atoms in the discharge. The overall positive ion density was observed to increase as argon flowrate is increased, and the electronegativity of the system decreases as a direct result of the increase in positive ion density, which increases the volume loss rate of negative ions.

## ACKNOWLEDGEMENT

The authors would like to thank D. B. Graves, A. J. Lichtenberg, and V. Vahedi for valuable discussions, suggestions, and criticisms throughout the preparation of this work. This work was supported in part by a grant from the Motorola Partnership in Research Program, grant W-7405-ENG-48 of the Plasma Physics Research Institute, Lawrence Livermore National Laboratory, NSF Grant ECS9217500 and DOE Grant DE-FG03-87ER13727.

## Appendix

Equations (13) and (14) are modified versions of the equations derived by Godyak and Maximov<sup>36</sup> and Lichtenberg et al<sup>37</sup>. For a plane parallel discharge, Godyak and Maximov<sup>36</sup> have determined the ratio of sheath edge to center ion density,  $n_s/n_0$ ,

$$h_{LO} = \frac{0.86}{\left(3 + \frac{L}{2\lambda}\right)^{1/2}} \quad (\text{A.1})$$

For an infinitely long cylindrical discharge, they give a similar result,

$$h_{RO} = \frac{0.8}{\left(4 + \frac{R}{\lambda}\right)^{1/2}} \quad (\text{A.2})$$

Here  $L$  and  $R$  are the chamber length and radius, and  $\lambda$  is the ion mean free path. Equations (A.1) and (A.2) are valid for electropositive discharges in the low to intermediate pressure regime, where  $2\lambda L \geq T_i/T_e$  and  $\lambda R \geq T_i/T_e$ , respectively. For the discharges of interest,  $\text{Cl}_2$  in particular, the plasma can become electronegative even at low pressures, especially if the surface recombination coefficient  $\gamma_{rec}$  for generation of  $\text{Cl}_2$  from  $\text{Cl}$  exceeds 0.1. Therefore, we generalize Eqs. (A.1) and (A.2) to include transitions from electropositive to electronegative regions, and extend the results into the regime of higher pressures.

We use the 1-D analytical oxygen model developed by Lichtenberg et al<sup>37</sup>. These authors showed that in a plane parallel geometry, with one kind of positive ion and one kind of negative ion, the plasma is composed of three regions: i) an electronegative (EN) region, where  $n_- \gg n_e$ , which is confined to the center of the discharge; ii) two electropositive (EP) regions, with  $n_- \ll n_e$ , which develop between the EN region and the two sheath edges; and iii) two thin sheath regions, where  $n_+ \gg n_e$  and there are no negative ions. The negative ion density profile is found to be approximately parabolic, and the relation between the width of the EN region,  $2l$ , and the chamber length  $L = 2l_p$ , is found to be

$$l^2 = \frac{2\alpha_0}{\gamma + 2\alpha_0} \left( \frac{2\gamma D l_p}{u_B} + l_p^2 \right) \quad (\text{A.3})$$

where  $\alpha_0$  is the ratio of negative ion to electron density at the center of the discharge,  $n_-/n_{e0}$ ,  $\gamma = T_e/T_i$ , and  $D = eT_i/M_i\nu_i$  is the positive (and negative) ion diffusion coefficient, with  $\nu_i$  the ion-neutral collision frequency. The first term in parentheses on the RHS of Eq. (A.3) is generally negligible; hence  $l \sim l_p$  for  $\alpha_0 \gg 1$ , and the EN region fills the entire volume, as shown in Fig. 1c. In this case, the electron density  $n_e$  is approximately constant over the entire volume. From the expressions derived by Lichtenberg et al<sup>37</sup>, the sheath edge density can be expressed as a function of  $\alpha_0$ .

$\gamma$ , and  $l_p$ ,

$$n_s = n_{e0} \left( 1 + \frac{2\alpha_0}{\gamma} \right) \left( \frac{1}{1 + \frac{l_p \mu_B}{2\gamma D}} \right), \quad (\text{A.5})$$

and from charge neutrality,

$$n_{i0} = n_{e0} (1 + \alpha_0), \quad (\text{A.6})$$

the  $h_L$  factor is found to be

$$h_{L0} = \frac{n_s}{n_0} = \frac{1 + \frac{2\alpha_0}{\gamma}}{1 + \alpha_0} \frac{1}{1 + \frac{l_p \mu_B}{2\gamma D}}. \quad (\text{A.7})$$

Note that for electropositive discharges,  $\alpha_0$  is zero, and  $h_L$  becomes

$$h_{L0} = \frac{1}{1 + \frac{l_p \mu_B}{2\gamma D}}, \quad (\text{A.8})$$

which is similar to the high pressure diffusion solution for a plane parallel discharge, with a cosine density distribution. For this system, using the Bohm flux condition at the sheath edge, the  $h_L$  factor can be shown to be approximately

$$h_{L0} = \frac{1}{\left( 1 + \left( \frac{2l_p \mu_B}{\pi\gamma D} \right)^2 \right)^{1/2}}. \quad (\text{A.9})$$

Equations (A.8) and (A.9) are only valid for high pressures, where  $l_p \mu_B / \gamma D \gg 1$ . The factor of 2 in Eq. (A.8) instead of  $\pi/2$  in Eq. (A.9) is due to the difference between the parabolic profile assumption and the cosine solution. Heuristically matching Eqs. (A.1), (A.7), and (A.9), we obtained a general  $h_L$  factor that can be used for transitions from low to high pressure and from

electropositive to electronegative regimes,

$$h_{L0} = \frac{1 + \frac{2\alpha_0}{\gamma}}{1 + \alpha_0} \frac{0.86}{\left(3 + \frac{L}{2\lambda} + \left(\frac{0.86Lu_B}{\pi\gamma D}\right)^2\right)^{1/2}} \quad [A.10]$$

where  $L = 2l_p$ . Since the global model does not include spatial variations, we approximate  $\alpha_0$  as  $(3/2) \alpha_{avg}$  from the assumption of the parabolic profile. As shown by Lichtenberg et al<sup>37</sup>, this approximation works well for large values of  $\alpha_0$ . For small  $\alpha_0$ , the negative ion density is small and the averaging procedure is not important. In Eq. (A.10), the peak ion density,  $n_0$ , must be modified in order to be consistent with the averaged density determined by the global model. Using the parabolic approximation,  $n_0 = (3/2) n_i$ , and  $\alpha_0 = (3/2) \alpha_{avg}$ , we approximate the leading term in Eq. (A.10) by

$$\frac{1 + \frac{3\alpha_{avg}}{\gamma}}{1 + \alpha_{avg}}$$

Hence the  $h_L$  factor now becomes the ratio of the sheath edge density  $n_{si}$  to the average bulk density  $n_i$ .

The derivation presented in this section is based on the assumption that there is only one type of positive ions present. For multiple ions, Eq. (A.10) is valid if we make the assumption that the ratio of the sheath edge density to the bulk density is independent of the type of ion. A similar treatment can be performed in the radial direction, in which we obtain  $h_R$  to be

$$h_R = \frac{n_{si}}{n_i} \Big|_{radial} = \frac{1 + \frac{3\alpha_{avg}}{\gamma}}{1 + \alpha_{avg}} \frac{0.8}{\left(4 + \frac{R}{\lambda} + \left(\frac{0.8Ru_B}{2.405J_1(2.405)\gamma D}\right)^2\right)^{1/2}} \quad [A.11]$$

We can see that in the limit of an electropositive low pressure discharge, where  $\alpha_{avg}$  and  $Ru_B/\gamma D \ll 1$ , Eq. (A.11) reduces to Eq. (A.2), and we get back the expression derived by Godyak and Maximov<sup>36</sup>.

## Figure Captions

Figure 1. Description of model; (a) schematic of reactor geometry used in the model; (b) density profiles for an electropositive discharge; (c) density profiles for an electronegative discharge.

Figure 2. Collisional energy loss per electron-ion pair created vs.  $T_e$ . Note differences between molecular gases of  $O_2$ ,  $Cl_2$  and atomic species Ar, O, and Cl.

Figure 3. Electron temperature  $T_e$  vs. pressure for the three systems of Ar,  $O_2$ , and  $Cl_2$ . Absorbed power = 1000 W,  $Q = 35$  SCCM,  $\gamma_{rec} = 0.0$ .

Figure 4. Total positive ion density  $n_+$  vs. pressure. Conditions are the same as Fig. 2.

Figure 5a. Ratio  $n_-/n_e$  of negative ions to electrons vs.  $\gamma_{rec}$  for an oxygen discharge. Absorbed power = 1000 W,  $Q = 35$  SCCM.

Figure 5b. Ratio  $n_-/n_e$  of negative ions to electrons vs.  $\gamma_{rec}$  for a chlorine discharge. Conditions are the same as Fig. 5a.

Figure 6a. Total positive ion density  $n_+$  vs  $\gamma_{rec}$  for  $O_2$ . Conditions are the same as Fig. 5a.

Figure 6b. Total positive ion density  $n_+$  vs  $\gamma_{rec}$  for  $Cl_2$ . Conditions are the same as Fig. 5a.

Figure 7a. Fractional dissociation vs  $\gamma_{rec}$  for  $O_2$ . Conditions are the same as Fig. 5a.

Figure 7b. Fractional dissociation vs  $\gamma_{rec}$  for  $Cl_2$ . Conditions are the same as Fig. 5a.

Figure 8. Comparison with experimental data for argon discharges. Curves are model results based on corresponding operating conditions and reactor geometry. Ra et al<sup>22</sup> (..... model, ◆ experiment); Mahoney et al<sup>23</sup> (..... model, ■ experiment); Oomori et al<sup>24</sup> (—— model, ● experiment).

Figure 9. Comparison with experimental data for chlorine discharges. Curves are model results based on corresponding operating conditions and reactor geometry. Ra et al<sup>22</sup> (..... model,  $\gamma_{rec} = 0$ , ..... model,  $\gamma_{rec} = 0.1$ , ■ experiment); Oomori et al<sup>24</sup> (—— model,  $\gamma_{rec} = 0$ , ..... model,  $\gamma_{rec} = 0.1$ , ● experiment).

Figure 10. Fraction of  $Ar^+$  vs fraction of argon in the feed gas. Absorbed power = 1000 W, total flowrate = 35 SCCM,  $\gamma_{rec} = 0.0$ .

Figure 11. Fraction of O atom density vs fraction of argon in the feed gas. Absorbed power = 1000 W, total flowrate = 35 SCCM,  $\gamma_{rec} = 0.0$ .

## REFERENCES

- <sup>1</sup> Park, S. K. and D. J. Economou, *J. Appl. Phys.* **68**(8), 3904, (1988).
- <sup>2</sup> Meyyappan, M., *J. Appl. Phys.* **71**(6), 2574, (1992).
- <sup>3</sup> Meyyappan, M. and T. R. Govindan, *J. Vac. Sci. Technol. A* **10**(4), 1344, (1992).
- <sup>4</sup> Meyyappan, M. and T. R. Govindan, *IEEE Trans. Plasma Sci.* **19**(2), 122, (1991).
- <sup>5</sup> Aydil, E. S. and D. J. Economou, *J. Electrochem. Soc.*, **139**(5), 1396, (1992).
- <sup>6</sup> Rogoff, G. L., J. M. Kramer, and R. B. Piejak, *IEEE Trans. Plasma Sci.*, **14**(2), 103, (1986).
- <sup>7</sup> Bassett, N. L. and D. J. Economou, *J. Appl. Phys.* **75**(4), 1931, (1994).
- <sup>8</sup> Vender, D., E. Stoffels, W. W. Stoffels, G.M.W. Kroesen, and F. J. de Hoog, 46th GEC, Montreal (1993).
- <sup>9</sup> Stoffels, E., W. W. Stoffels, D. Vender, G.M.W. Kroesen, and F. J. de Hoog, 46th GEC, Montreal (1993).
- <sup>10</sup> Lee, C., D. B. Graves, M. A. Lieberman, and D. W. Hess, *J. Electrochem. Soc.* **141**(6), 1994.
- <sup>11</sup> Lieberman, M.A., and R. A. Gottscho, in *Physics of Thin Films*, ed. by M. Francombe and J. Vossen, Academic Press, Vol. 18, 1994.
- <sup>12</sup> Gottscho, R. A., G. R. Scheller, T. Intrator, and D. B. Graves, *J. Vac. Sci. Technol. A* **6**(3), 1393, (1988).
- <sup>13</sup> Scheller, G. R., R. A. Gottscho, T. Intrator, and D. B. Graves, *J. Appl. Phys.*, **64**(9), 4384, (1988).
- <sup>14</sup> Scheller, G. R., R. A. Gottscho, D. B. Graves, and T. Intrator, *J. Appl. Phys.*, **64**(2), 598, (1988).
- <sup>15</sup> Ivanov, V. A. and I. V. Makasyuk, *Opt. Spectroc. (USSR)*, **72**(2), 159, (1992).

- <sup>16</sup>Nakano, T. N. Sadeghi, and R. A. Gottscho, *Appl. Phys. Lett.* **58**, 458 (1991).
- <sup>17</sup>Sadeghi, N., T. Nakano, D. J. Trevor, and R. A. Gottscho, *J. Appl. Phys.* **70**, 2552 (1991).
- <sup>18</sup>Bird, R. B., W. E. Stewart, and E. N. Lightfoot, *Transport Phenomena*, p. 511, John Wiley & Sons, Inc., New York (1960).
- <sup>19</sup>Kiss, L. D. B. and H. H. Sawin, *J. Electrochem. Soc.*, **139**(5), 1414, (1992).
- <sup>20</sup>Greaves, J. C., and J. W. Linnett, *Trans. Farad. Soc.*, **55**, 1355 (1959).
- <sup>21</sup>Coburn, J. W., *J. Vac. Sci. Technol.* **B 12**, to be published in May/June issue, 1994.
- <sup>22</sup>Ra Y., S. G. Bradley, and C. H. Chen, submitted to *J. Vac. Sci. Technol.*
- <sup>23</sup>Mahoney, L. J., A. E. Wendt, E. Barriros, C. J. Richards, and J. L. Shohet, submitted to *J. Appl. Phys.*
- <sup>24</sup>Oomori, T., M. Tuda, H. Ootera, and K. Ono, *J. Vac. Sci. Technol. A* **9**(3), 722, (1991).
- <sup>25</sup>Margreiter, D., H. Deutsch, and T. D. Mark, *Contrib. Plasma Phys.* **30** (4), 487, (1990).
- <sup>26</sup>Rapp, D. and P. Englander-Golden, *J. Chem Phys.*, **43**(5), 1464, (1965).
- <sup>27</sup>Peterson, L. R., and J. E. Allen, Jr., *J. Chem. Phys.*, **56**(12), 6068, (1972).
- <sup>28</sup>Rebrion, C., B. R. Rowe, and J. B. Marquette, *J. Chem. Phys.*, **91**(10), 6142, (1989).
- <sup>29</sup>Dotan, I., and A. A. Viggiano, *Chem. Phys. Lett.*, **209**(1-2), 67, (1993).
- <sup>30</sup>Massey, H. S. W., "Negative Atomic Ions", *Proc. Roy. Soc. (London)* **155A**, 472 (1936).
- <sup>31</sup>Lennon, M. A., K. L. Bell, H. B. Gilbody, J. G. Hughes, A. E. Kingston, M. J. Murray, and F. J. Smith, *J. Phys. Chem. Ref. Data*, **17**(3), 1285, (1988).
- <sup>32</sup>Rescigno, T. N., Lawrence Livermore National Laboratory, submitted to *Phys. Rev. A*.
- <sup>33</sup>Ganas, P. S., *J. Appl. Phys.*, **63**, 277 (1988).
- <sup>34</sup>Kurepa, M. V., and d. S. Belie, *J. Phys. B., Atom, Molec. Phys.*, **11**(21), 3719, (1978).
- <sup>35</sup>Cosby, P. C., and H. Helm, SRI Report, PYU 1147/MP 92-280, (1992).
- <sup>36</sup>Godyak, V. A., *Soviet Radio Frequency Discharge Research*, Chapter 5, Delphic Associates, Inc., 1986.

<sup>37</sup>Lichtenberg, A. J., V. Vahedi, M. A. Lieberman, and T. Rognlien, *J. Appl. Phys.*, **75**(5), 2339, (1994).

<sup>38</sup>Rebrion, C., B. R. Rowe, and J. B. Marquette, *J. Chem. Phys.*, **91**(10), 6142, (1989).

<sup>39</sup>Kushner, M.J. *J. Appl. Phys.*, **71**(9), 4173, (1992).

**Table 1. Oxygen Reaction Set**

Reaction		Rate Coefficients	Reference
e + O <sub>2</sub>	-----> O <sub>2</sub> <sup>+</sup> + 2e	$k_1 = 9.0 \times 10^{-10} (T_e)^2 \exp(-12.6 / T_e) \text{ cm}^3\text{-s}^{-1}$	10
e + O <sub>2</sub>	-----> O( <sup>3</sup> P) + O( <sup>1</sup> D) + e	$k_2 = 5.0 \times 10^{-8} \exp(-8.4 / T_e) \text{ cm}^3\text{-s}^{-1}$	10
e + O <sub>2</sub>	-----> O( <sup>3</sup> P) + O <sup>-</sup>	$k_3 = 4.6 \times 10^{-11} \exp(2.91 / T_e - 1.26 / T_e^2 + 6.92 / T_e^3) \text{ cm}^3\text{-s}^{-1}$	10
e + O( <sup>3</sup> P)	-----> O <sup>+</sup> + 2e	$k_4 = 9.0 \times 10^{-9} (T_e)^{0.7} \exp(-13.6 / T_e) \text{ cm}^3\text{-s}^{-1}$	10
O <sup>-</sup> + O <sub>2</sub> <sup>+</sup>	-----> O( <sup>3</sup> P) + O <sub>2</sub>	$k_5 = 1.4 \times 10^{-7} \text{ cm}^3\text{-s}^{-1}$	10
O <sup>-</sup> + O <sup>+</sup>	-----> O( <sup>3</sup> P) + O( <sup>3</sup> P)	$k_6 = 2.7 \times 10^{-7} \text{ cm}^3\text{-s}^{-1}$	10
e + O <sup>-</sup>	-----> O( <sup>3</sup> P) + 2e	$k_7 = 1.73 \times 10^{-7} \exp(-5.67 / T_e + 7.3 / T_e^2 - 3.48 / T_e^3) \text{ cm}^3\text{-s}^{-1}$	10
e + O <sub>2</sub>	-----> O( <sup>3</sup> P) + O( <sup>3</sup> P) + e	$k_8 = 4.23 \times 10^{-9} \exp(-5.56 / T_e) \text{ cm}^3\text{-s}^{-1}$	10
e + O( <sup>3</sup> P)	-----> O( <sup>1</sup> D) + e	$k_9 = 4.47 \times 10^{-9} \exp(-2.286 / T_e) \text{ cm}^3\text{-s}^{-1}$	10
O( <sup>1</sup> D) + O <sub>2</sub>	-----> O( <sup>3</sup> P) + O <sub>2</sub>	$k_{10} = 4.1 \times 10^{-11} \text{ cm}^3\text{-s}^{-1}$	10
O( <sup>1</sup> D) + O( <sup>3</sup> P)	-----> O( <sup>3</sup> P) + O( <sup>3</sup> P)	$k_{11} = 8.1 \times 10^{-12} \text{ cm}^3\text{-s}^{-1}$	10
O( <sup>1</sup> D)	---(wall)-----> O( <sup>3</sup> P)	$k_{12} = D_{\text{eff}} / \Lambda^2 \text{ s}^{-1}$	10
e + O( <sup>1</sup> D)	-----> O <sup>+</sup> + 2e	$k_{13} = 9.0 \times 10^{-9} (T_e)^{0.7} \exp(-11.6 / T_e) \text{ cm}^3\text{-s}^{-1}$	a
O <sup>+</sup> (g)	---(wall)-----> O( <sup>3</sup> P) (g)	$k_{14} = 2u_{B,O^+} (R^2 h_L + RLh_R) / R^2 L \text{ s}^{-1}$	b
O <sub>2</sub> <sup>+</sup> (g)	---(wall)-----> O <sub>2</sub> (g)	$k_{15} = 2u_{B,O_2^+} (R^2 h_L + RLh_R) / R^2 L \text{ s}^{-1}$	b
O (g)	---(wall)-----> 1/2 O <sub>2</sub> (g)	$k_{16} = \gamma_{\text{rec}} D_{\text{eff}} / \Lambda^2 \text{ s}^{-1}$	

$T_e [=] \text{ eV}$

a. This rate coefficient is estimated from  $k_4$ , where the same process takes place except that the threshold energy is 13.6 eV instead of 11.6 eV.

b. These surface loss rate coefficients are estimated from the diffusion of ions to the walls (see Appendix).

**Table 2. Chlorine Reaction Set**

Reaction	Rate Coefficients	Reference
$e + Cl_2 \longrightarrow Cl_2^+ + 2e$	$k_1 = 9.21 \times 10^{-8} \exp(-12.9 / T_e) \text{ cm}^3\text{-s}^{-1}$	34
$e + Cl_2 \longrightarrow Cl^+ + Cl + 2e$	$k_1 = 3.88 \times 10^{-9} \exp(-15.5 / T_e) \text{ cm}^3\text{-s}^{-1}$	34
$e + Cl_2 \longrightarrow Cl^+ + Cl^- + e$	$k_1 = 8.55 \times 10^{-10} \exp(-12.65 / T_e) \text{ cm}^3\text{-s}^{-1}$	34
$e + Cl_2 \longrightarrow 2Cl(^2P) + e$	$k_2 = 3.80 \times 10^{-8} \exp(-3.824 / T_e) \text{ cm}^3\text{-s}^{-1}$	35
$e + Cl_2 \longrightarrow Cl(^2P) + Cl^-$	$k_3 = 3.69 \times 10^{-10} \exp(-1.68 / T_e + 1.457 / T_e^2 - 0.44 / T_e^3 + 0.0572 / T_e^4 - 0.0026 / T_e^5) \text{ cm}^3\text{-s}^{-1}$	34
$e + Cl(^2P) \longrightarrow Cl^+ + 2e$	$k_4 = (T_e/12.96)^{0.5} \exp(-12.96 / T_e) (1.419 \times 10^{-7} - 1.864 \times 10^{-8} \log(T_e/12.96) - 5.439 \times 10^{-8} \log(T_e/12.96)^2 + 3.306 \times 10^{-8} \log(T_e/12.96)^3 - 3.54 \times 10^{-9} \log(T_e/12.96)^4 - 2.915 \times 10^{-8} \log(T_e/12.96)^5) \text{ cm}^3\text{-s}^{-1}$	31
$Cl^- + Cl_2^+ \longrightarrow Cl(^2P) + Cl_2$	$k_5 = 5.0 \times 10^{-8} \text{ cm}^3\text{-s}^{-1}$	6
$Cl^- + Cl^+ \longrightarrow Cl(^2P) + Cl(^2P_u)$	$k_6 = 5.0 \times 10^{-8} \text{ cm}^3\text{-s}^{-1}$	6
$e + Cl^- \longrightarrow Cl(^2P) + 2e$	$k_7 = 2.63 \times 10^{-8} \exp(-5.37 / T_e) \text{ cm}^3\text{-s}^{-1}$	32
$Cl(^2P) \longrightarrow 1/2 Cl_2$	$k_{12} = \gamma_{rec} D_{eff} / \Lambda^2 \text{ s}^{-1}$	10
$Cl^+ \longrightarrow Cl(^2P)$	$k_{14} = 2u_{B,Cl^+} (R^2 h_L + RLh_R) / R^2 L \text{ s}^{-1}$	a
$Cl_2^+ \longrightarrow Cl_2(g)$	$k_{15} = 2u_{B,Cl_2^+} (R^2 h_L + RLh_R) / R^2 L \text{ s}^{-1}$	a

$T_e$  [=] eV

a. These surface loss rate coefficients are estimated from the diffusion of ions to the walls (see Appendix).

**Table 3. Argon Reaction Set**

Reaction		Rate Coefficients	Reference
e + Ar	-----> Ar <sup>+</sup> + 2e	$k_1 = 1.23 \times 10^{-7} \exp(-18.68 / T_e) \text{ cm}^3\text{-s}^{-1}$	26
e + Ar	-----> Ar* + e	$k_2 = 3.71 \times 10^{-8} \exp(-15.06 / T_e) \text{ cm}^3\text{-s}^{-1}$	27
e + Ar*	-----> Ar <sup>+</sup> + 2e	$k_3 = 2.05 \times 10^{-7} \exp(-4.95 / T_e) \text{ cm}^3\text{-s}^{-1}$	25
e + Ar*	-----> Ar + e	$k_4 = 2.0 \times 10^{-7} \text{ cm}^3\text{-s}^{-1}$	12-14
Ar* + Ar*	-----> Ar + Ar <sup>+</sup>	$k_5 = 6.2 \times 10^{-10} \text{ cm}^3\text{-s}^{-1}$	12-14
Ar <sup>+</sup>	-----> Ar	$k_6 = 2u_{B,Ar^+} (R^2 h_L + RLh_R) / R^2 L \text{ s}^{-1}$	a
Ar*	-----> Ar	$k_7 = D_{\text{eff}} / \Lambda^2 \text{ s}^{-1}$	10
$T_e$ [=] eV			

a. These surface loss rate coefficients are estimated from the diffusion of ions to the walls (see Appendix).

**Table 4. Energy Loss Reactions for Chlorine Molecules**

Reaction		Rate Coefficient	Reference
e + Cl <sub>2</sub>	-----> Cl <sub>2</sub> (b <sup>3</sup> Π <sub>u</sub> ) + e	k = 6.13 x 10 <sup>-10</sup> exp(2.74 / T <sub>e</sub> - 6.85 / T <sub>e</sub> <sup>2</sup> + 3.69 / T <sub>e</sub> <sup>3</sup> - 0.856 / T <sub>e</sub> <sup>4</sup> + 0.0711 / T <sub>e</sub> <sup>5</sup> ) cm <sup>3</sup> -s <sup>-1</sup>	32
	-----> Cl <sub>2</sub> (1 <sup>1</sup> Π <sub>u</sub> ) + e	k = 3.80 x 10 <sup>-8</sup> exp(-3.824 / T <sub>e</sub> ) cm <sup>3</sup> -s <sup>-1</sup>	32
	-----> Cl <sub>2</sub> (1 <sup>1</sup> Π <sub>g</sub> ) + e	k = 9.74 x 10 <sup>-9</sup> exp(-10.71 / T <sub>e</sub> ) cm <sup>3</sup> -s <sup>-1</sup>	32
	-----> Cl <sub>2</sub> (1 <sup>1</sup> Σ <sub>u</sub> ) + e	k = 2.12 x 10 <sup>-9</sup> exp(-11.16 / T <sub>e</sub> ) cm <sup>3</sup> -s <sup>-1</sup>	32
	-----> Cl <sub>2</sub> + e	k = 4.47 x 10 <sup>-7</sup> exp(-2.17 / T <sub>e</sub> + 0.362 / T <sub>e</sub> <sup>2</sup> - 0.0196 / T <sub>e</sub> <sup>3</sup> ) cm <sup>3</sup> -s <sup>-1</sup> (momentum transfer)	32
	-----> Cl <sub>2</sub> <sup>+</sup> + e	k = 9.21 x 10 <sup>-8</sup> exp(-12.9 / T <sub>e</sub> ) cm <sup>3</sup> -s <sup>-1</sup>	34
	-----> Cl <sub>2</sub> + e	k = 9.26 x 10 <sup>-10</sup> exp(5.85 / T <sub>e</sub> - 4.94 / T <sub>e</sub> <sup>2</sup> + 1.716 / T <sub>e</sub> <sup>3</sup> - 0.251 / T <sub>e</sub> <sup>4</sup> + 0.123 / T <sub>e</sub> <sup>5</sup> ) cm <sup>3</sup> -s <sup>-1</sup> (vibrational excitation)	32
	-----> 2Cl (2 <sup>2</sup> P) + e	k = 3.80 x 10 <sup>-8</sup> exp(-3.824 / T <sub>e</sub> ) cm <sup>3</sup> -s <sup>-1</sup>	35

**Table 5. Energy Loss Reactions for Chlorine Atoms**

Reaction	Process	Reference
$e + \text{Cl} (^2\text{P})$ -----> $\text{Cl} (^3\text{D}) + 2e$	$k = 1.99 \times 10^{-8} \exp(-10.06 / T_e) \text{ cm}^3\text{-s}^{-1}$	33
-----> $\text{Cl} (^4\text{D}) + e$	$k = 9.24 \times 10^{-9} \exp(-11.15 / T_e) \text{ cm}^3\text{-s}^{-1}$	33
-----> $\text{Cl} (^4\text{P}) + e$	$k = 1.60 \times 10^{-8} \exp(-10.29 / T_e) \text{ cm}^3\text{-s}^{-1}$	32
-----> $\text{Cl} (^4\text{S}) + e$	$k = 1.27 \times 10^{-8} \exp(-10.97 / T_e) \text{ cm}^3\text{-s}^{-1}$	33
-----> $\text{Cl} (^5\text{D}) + e$	$k = 5.22 \times 10^{-9} \exp(-11.12 / T_e) \text{ cm}^3\text{-s}^{-1}$	33
-----> $\text{Cl} (^5\text{P}) + e$	$k = 2.79 \times 10^{-9} \exp(-11.06 / T_e) \text{ cm}^3\text{-s}^{-1}$	32

**Table 6. Argon-Oxygen Reactions**

Reaction	Rate Coefficients	Reference
$O^- + Ar^+ \text{ -----> } Ar + O$	$k = 2.70 \times 10^{-7} \text{ cm}^3\text{-s}^{-1}$	a
$O_2 + Ar^* \text{ -----> } Ar + O_2$	$k = 1.12 \times 10^{-9} \text{ cm}^3\text{-s}^{-1}$	b
$O + Ar^* \text{ -----> } Ar + O$	$k = 8.10 \times 10^{-12} \text{ cm}^3\text{-s}^{-1}$	b
$O_2 + Ar^* \text{ -----> } Ar + O + O$	$k = 5.80 \times 10^{-11} \text{ cm}^3\text{-s}^{-1}$	c
$O_2 + Ar^+ \text{ -----> } O_2^+ + Ar$	$k = 1.20 \times 10^{-11} \text{ cm}^3\text{-s}^{-1}$	38
$O + Ar^+ \text{ -----> } O^+ + Ar$	$k = 1.20 \times 10^{-11} \text{ cm}^3\text{-s}^{-1}$	d

- a. The reaction rate was assumed to be identical to the  $O^-/O^+$  recombination rate.  
 b. Estimated from similar quenching reactions for  $Cl_2$  and  $N_2$  give in references 13, 14.  
 c. Estimated from similar reactions in  $NH_3$  given in reference 39.  
 d. Estimated to be the same as the  $O_2/Ar^+$  reaction obtained from reference 38.

Figure 1.

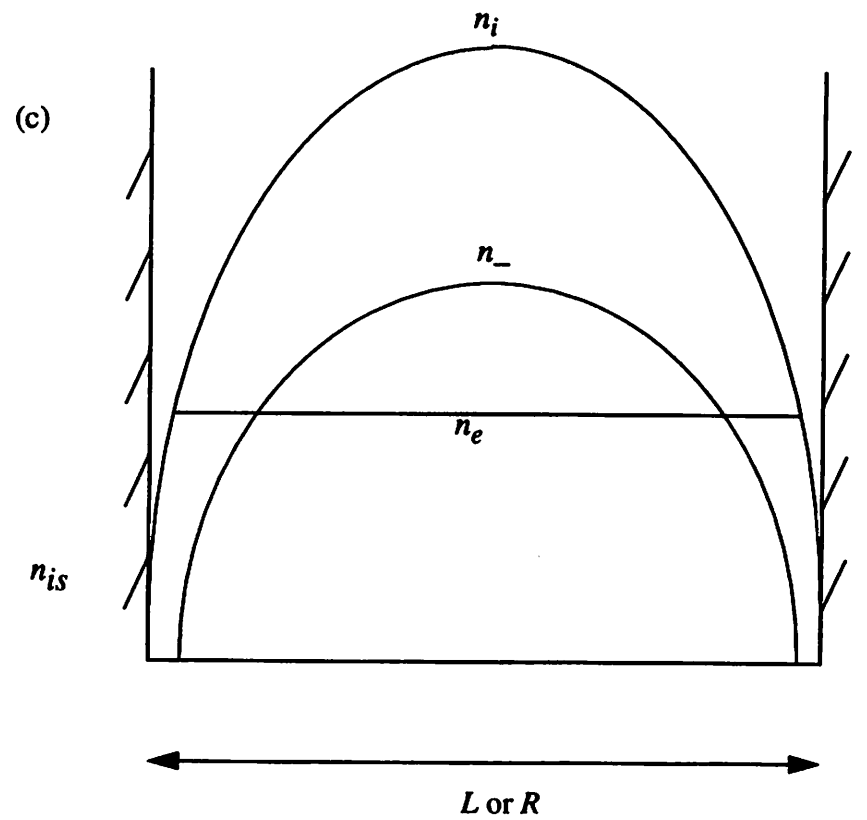
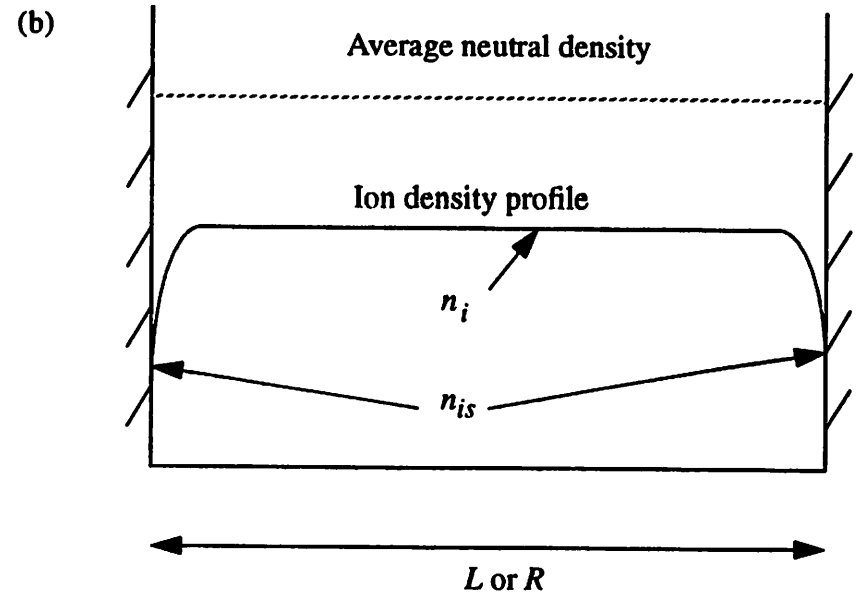
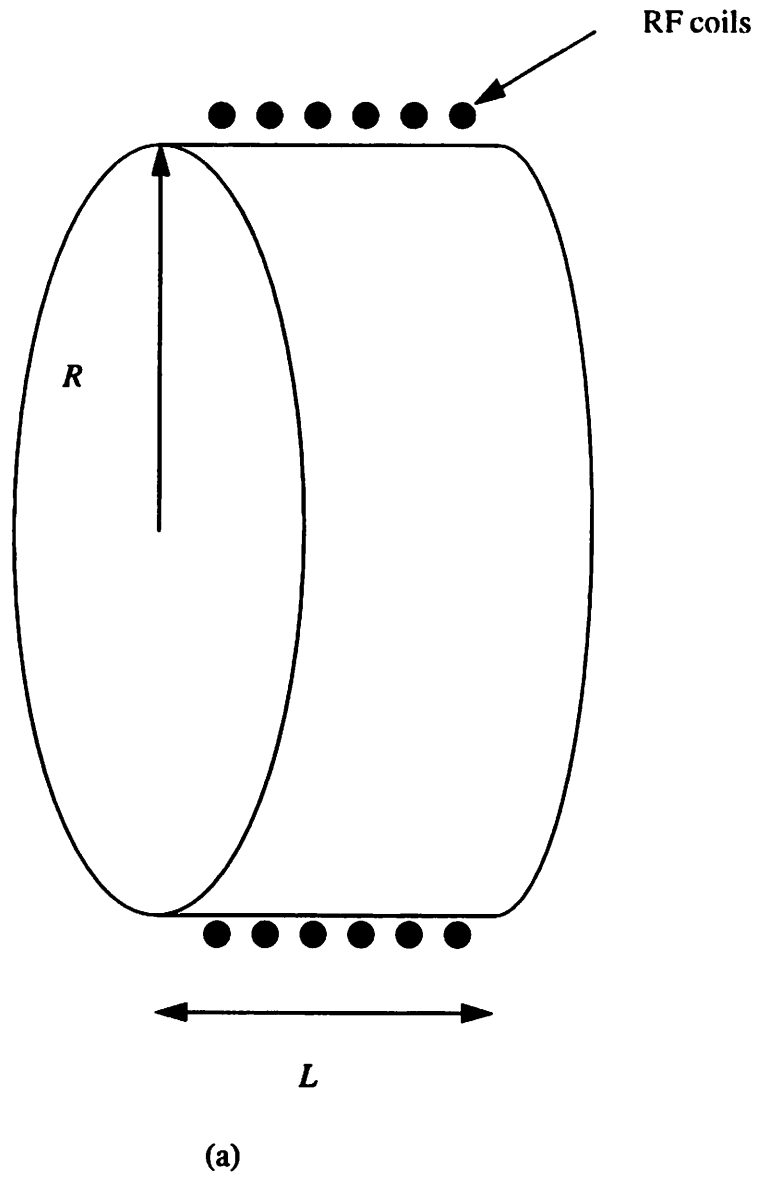


Fig. 2

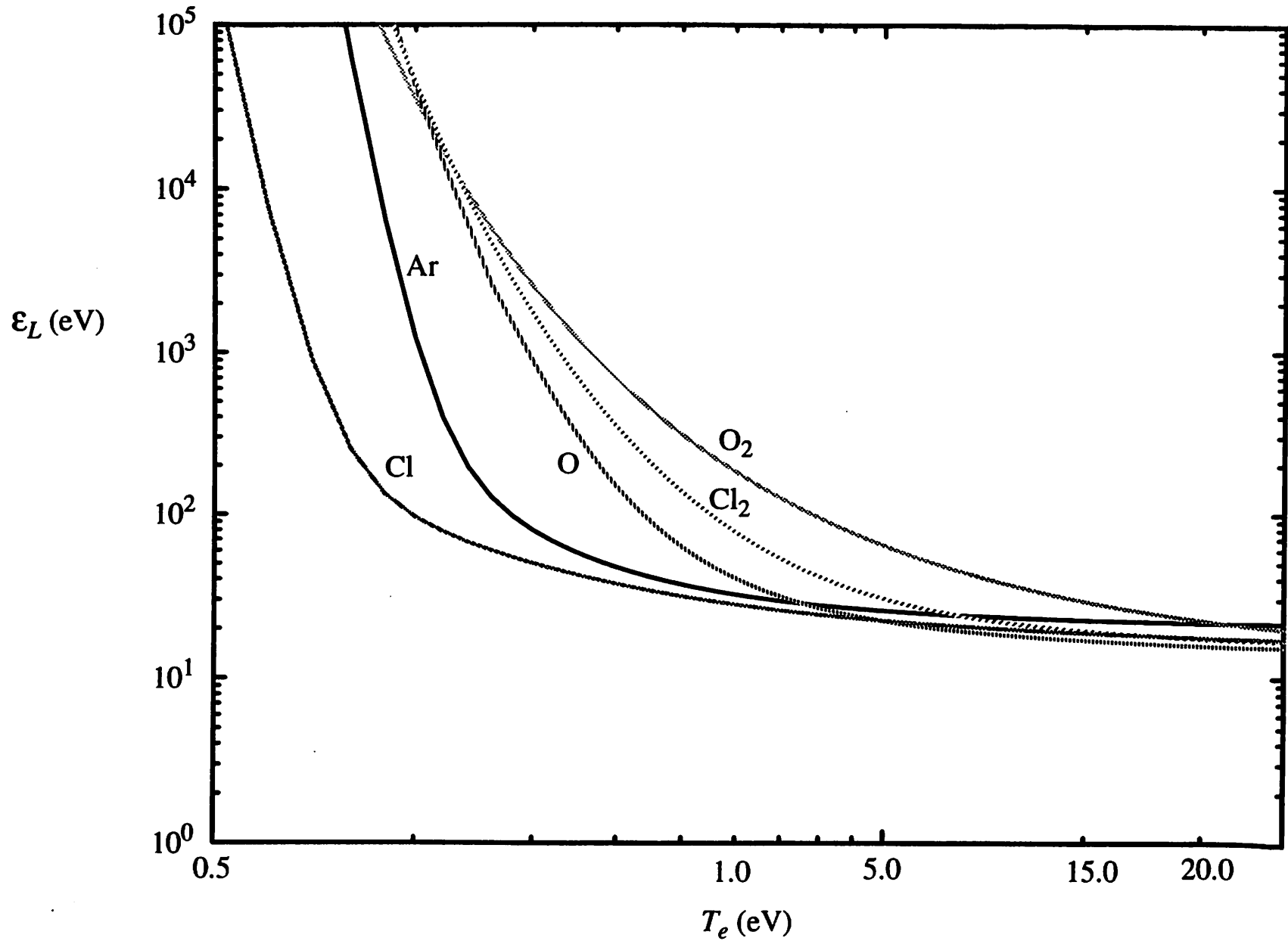


Fig 3

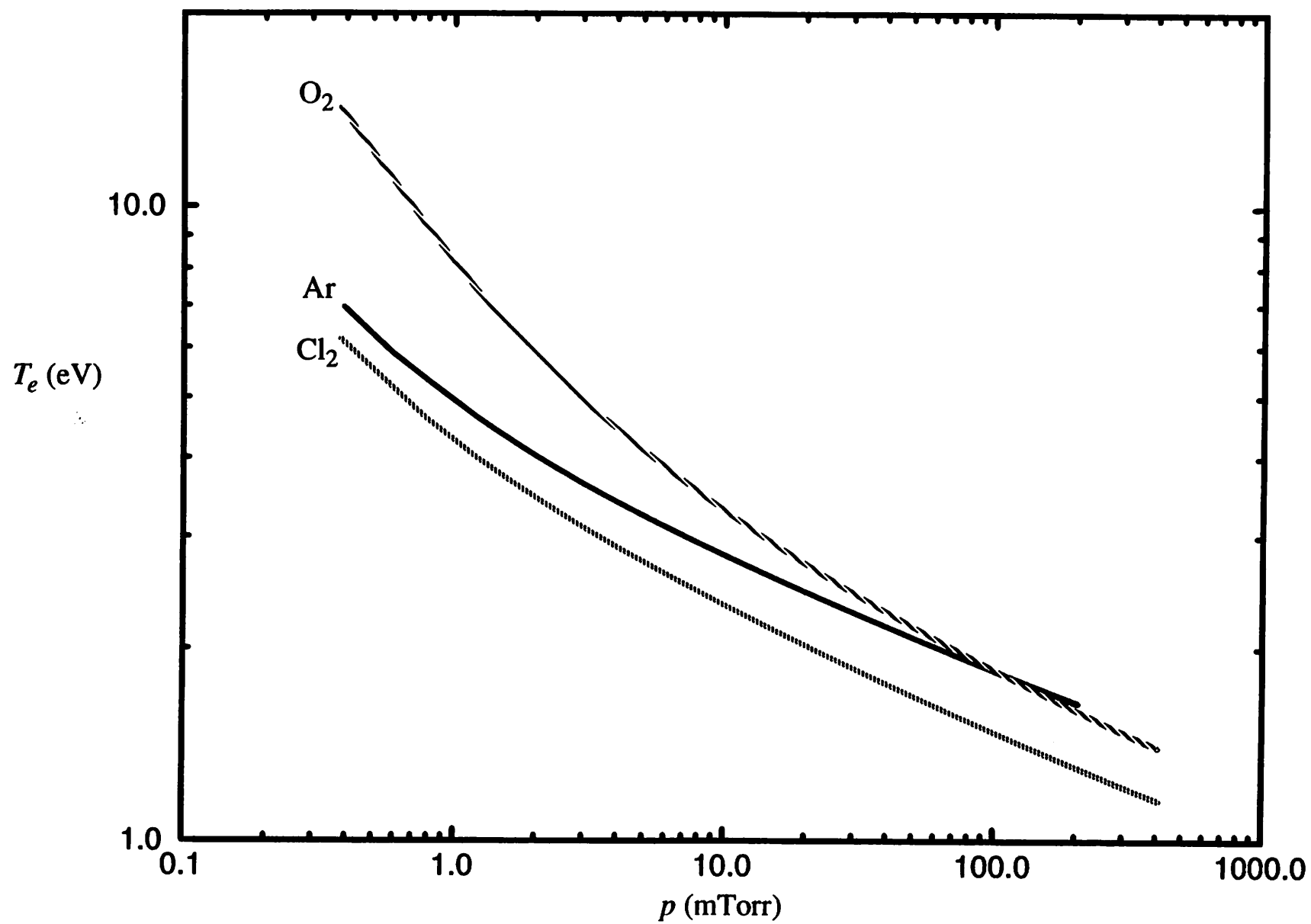


Fig. 4

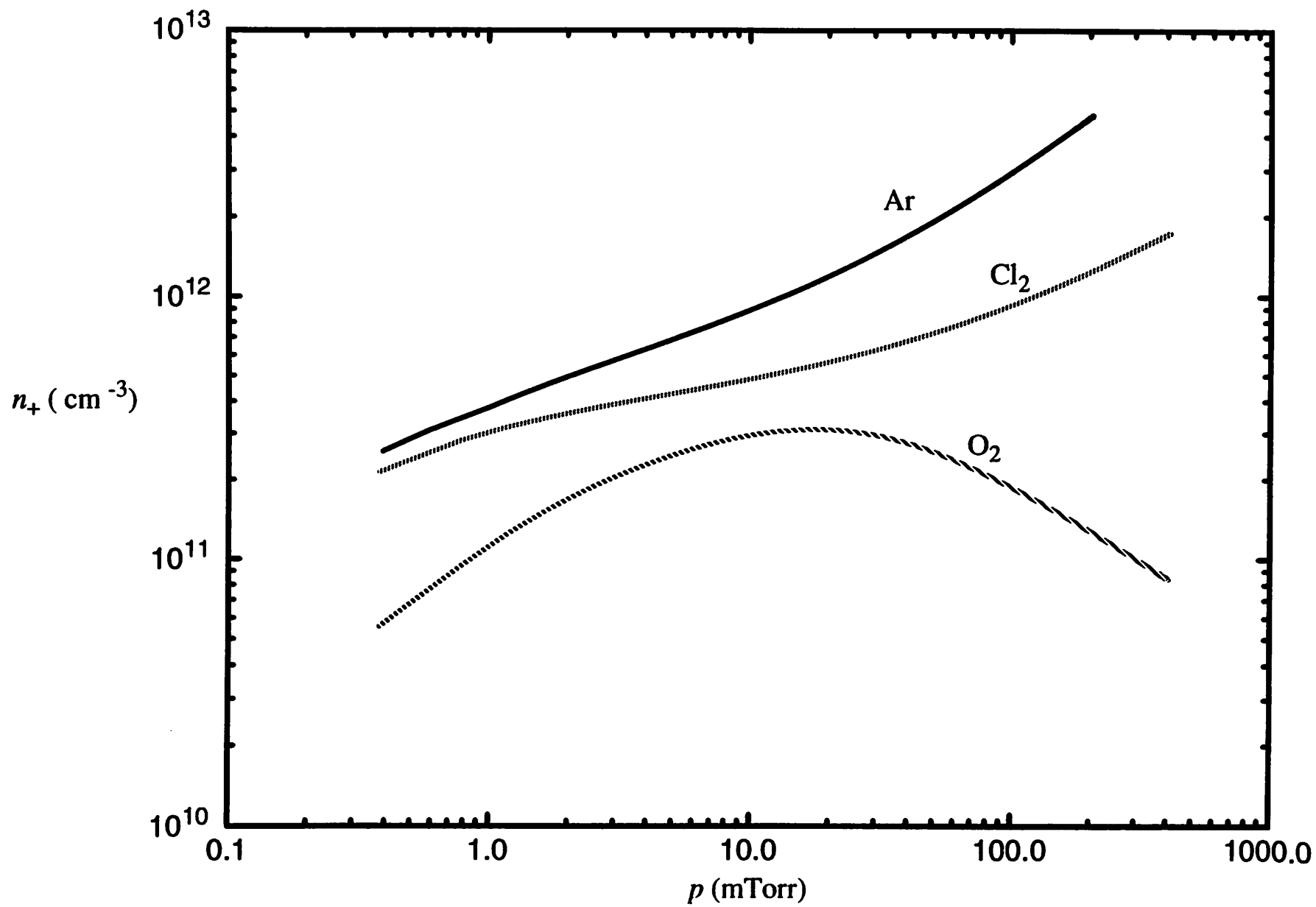


Fig 5a.

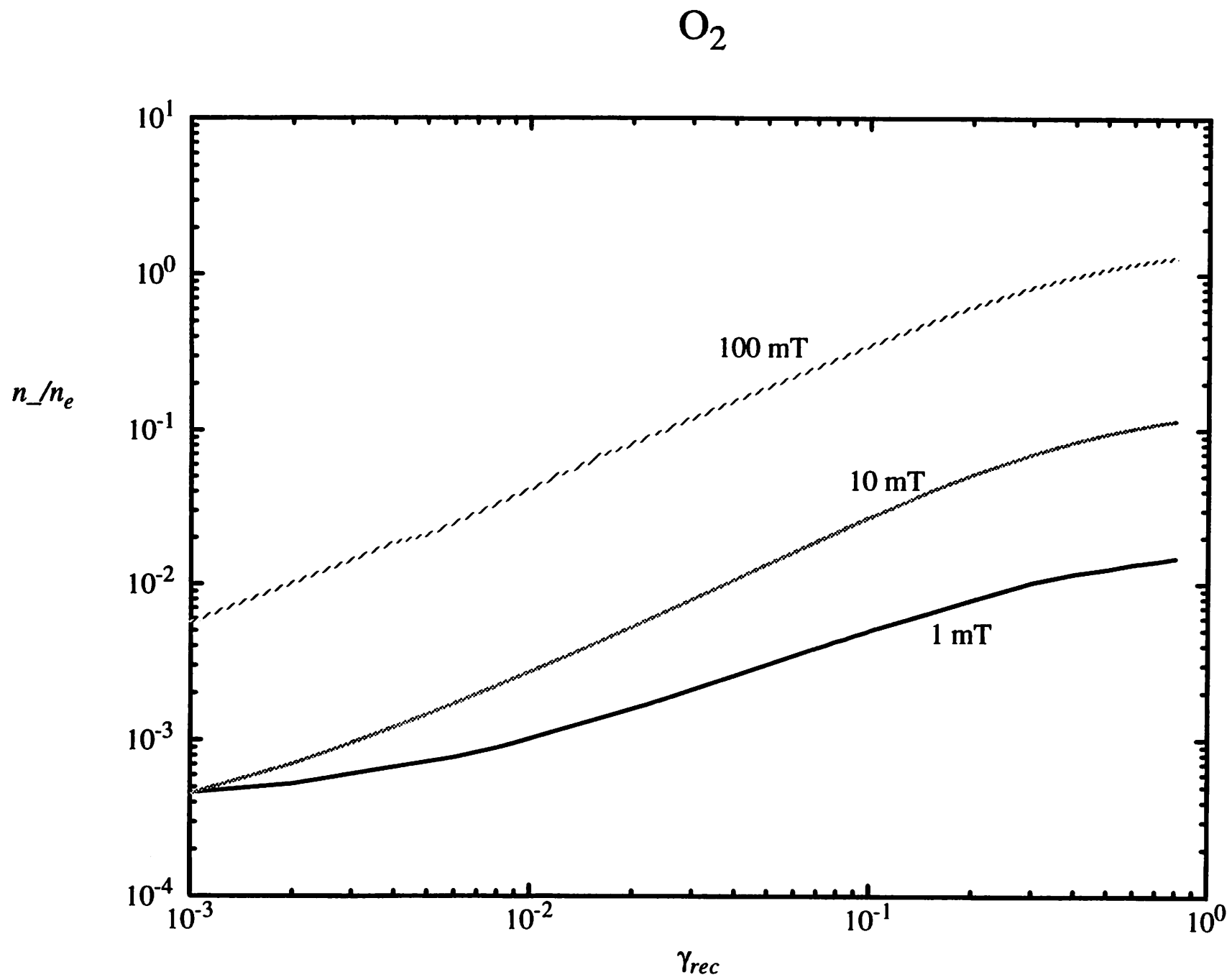


Fig 5b.

Cl<sub>2</sub>

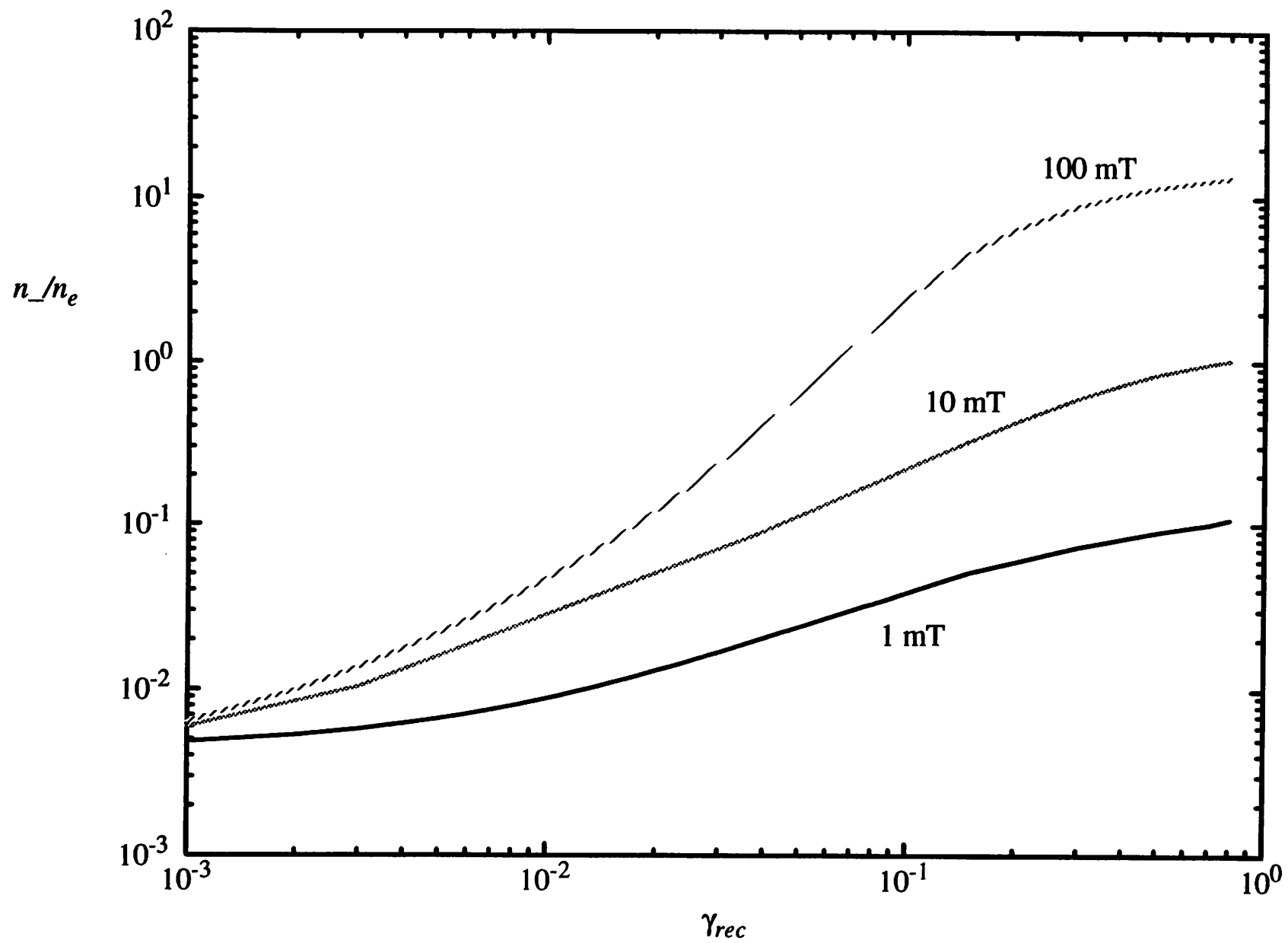


Fig. 6a.

O<sub>2</sub>

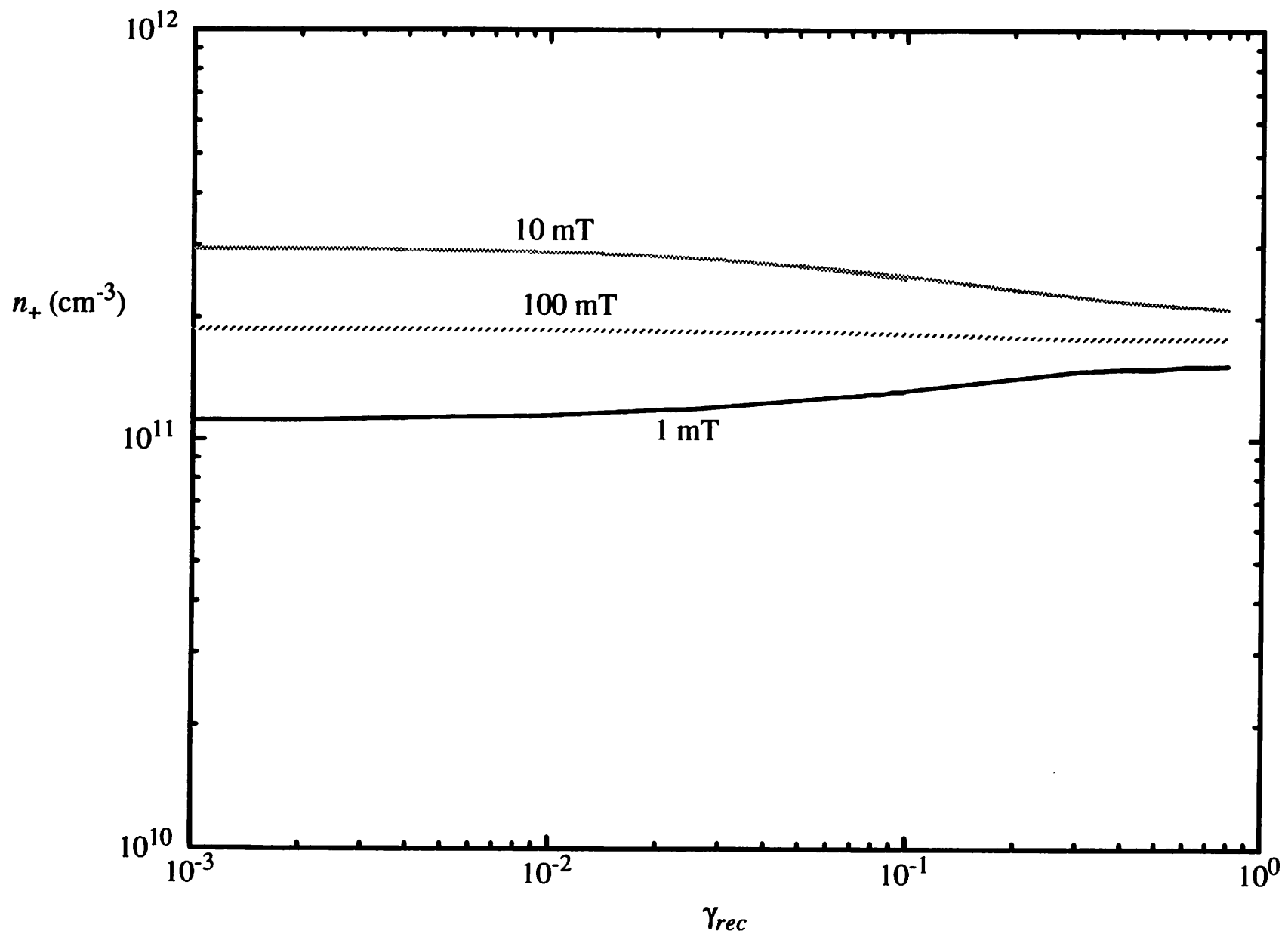


Figure 6b.

Cl<sub>2</sub>

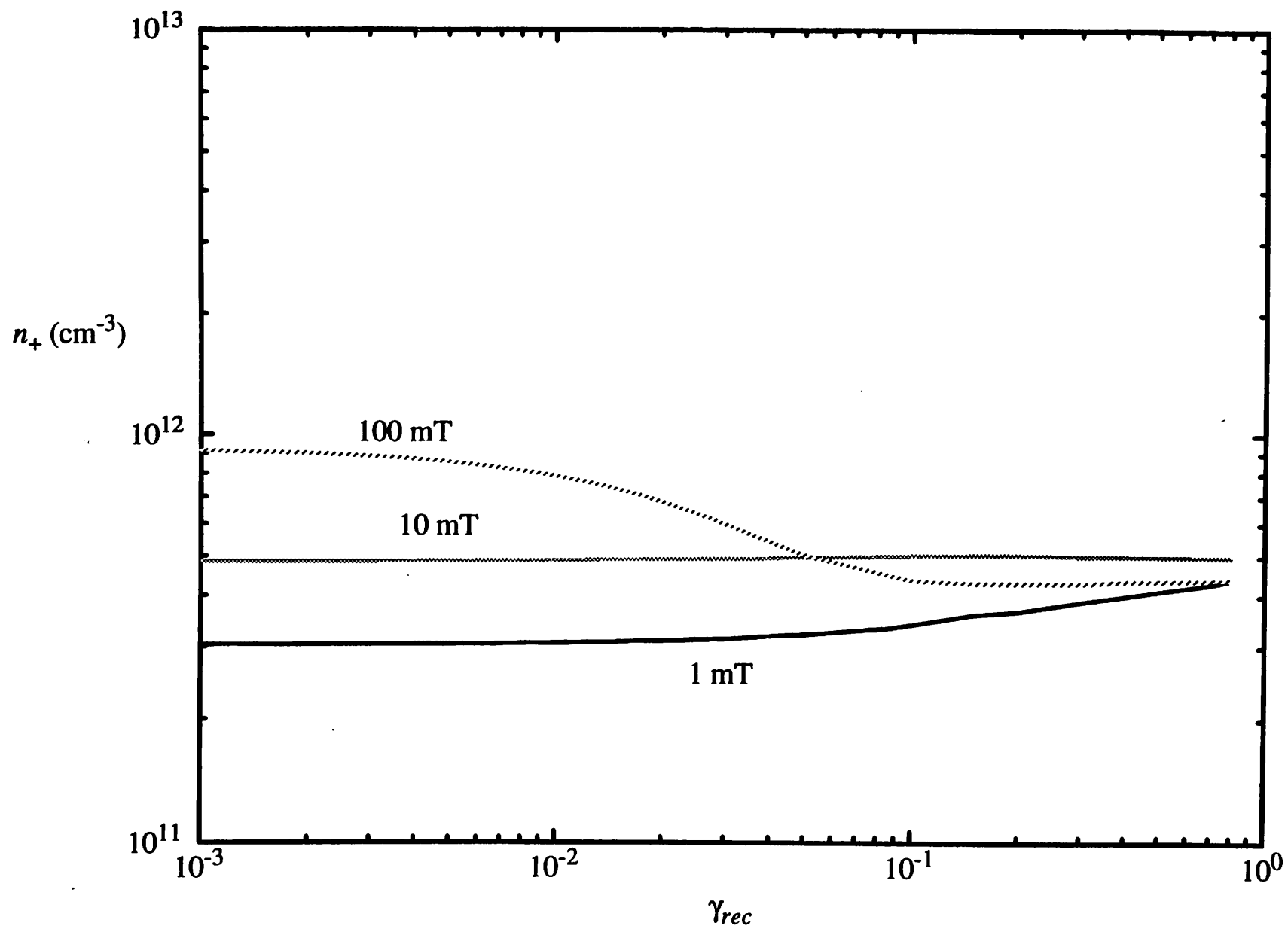


Fig 7a.

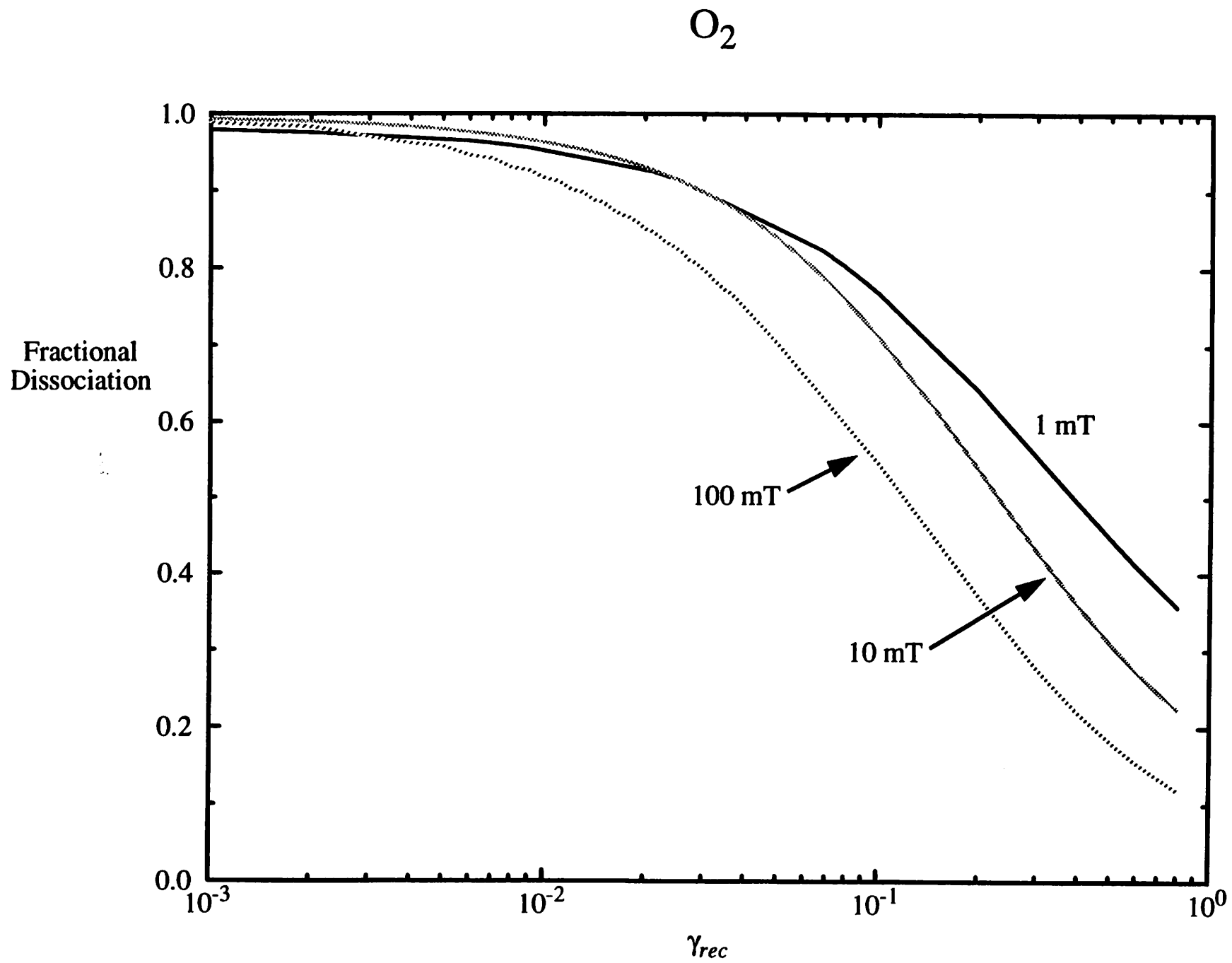


Fig 7b.

Cl<sub>2</sub>

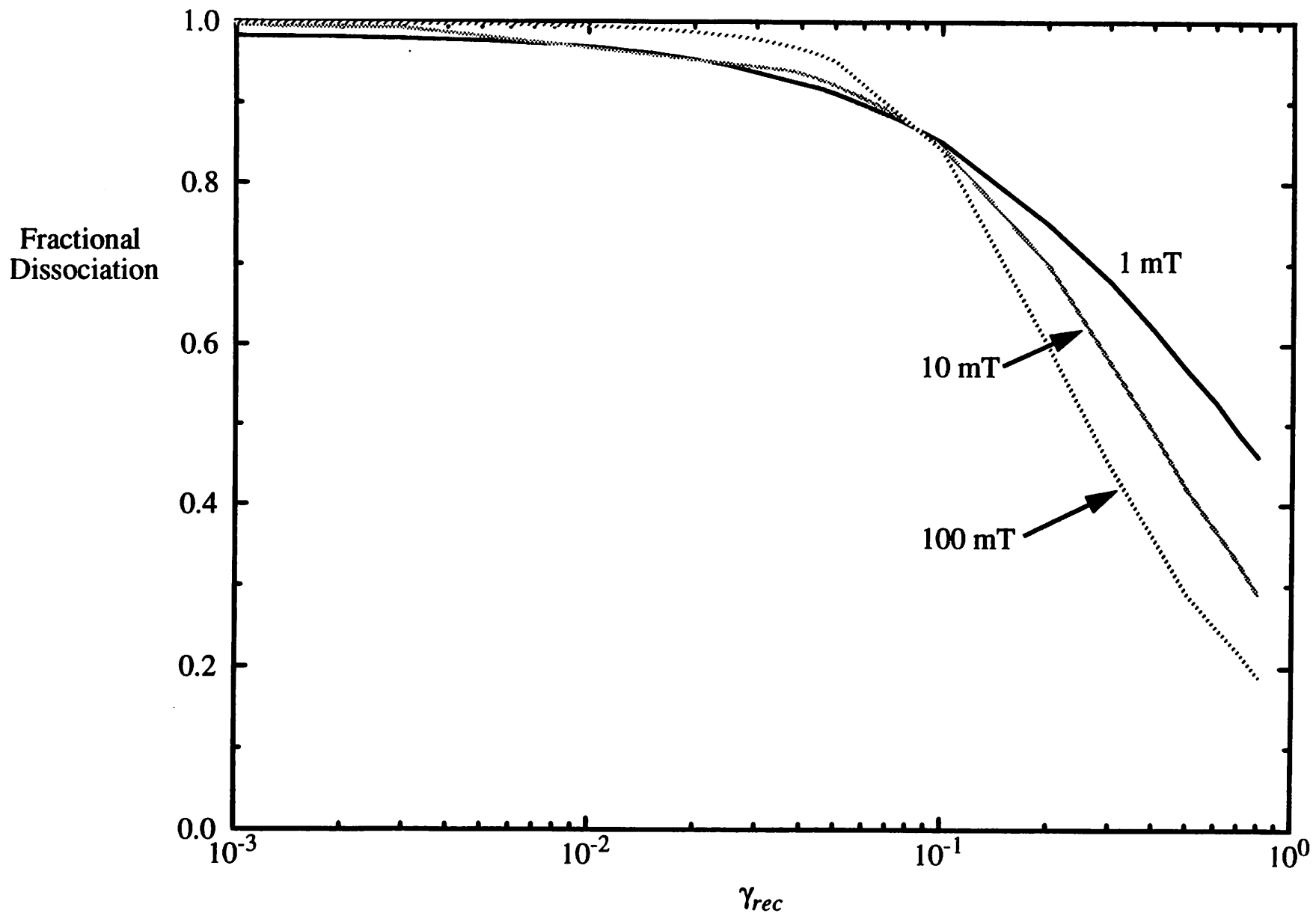


Figure 8.

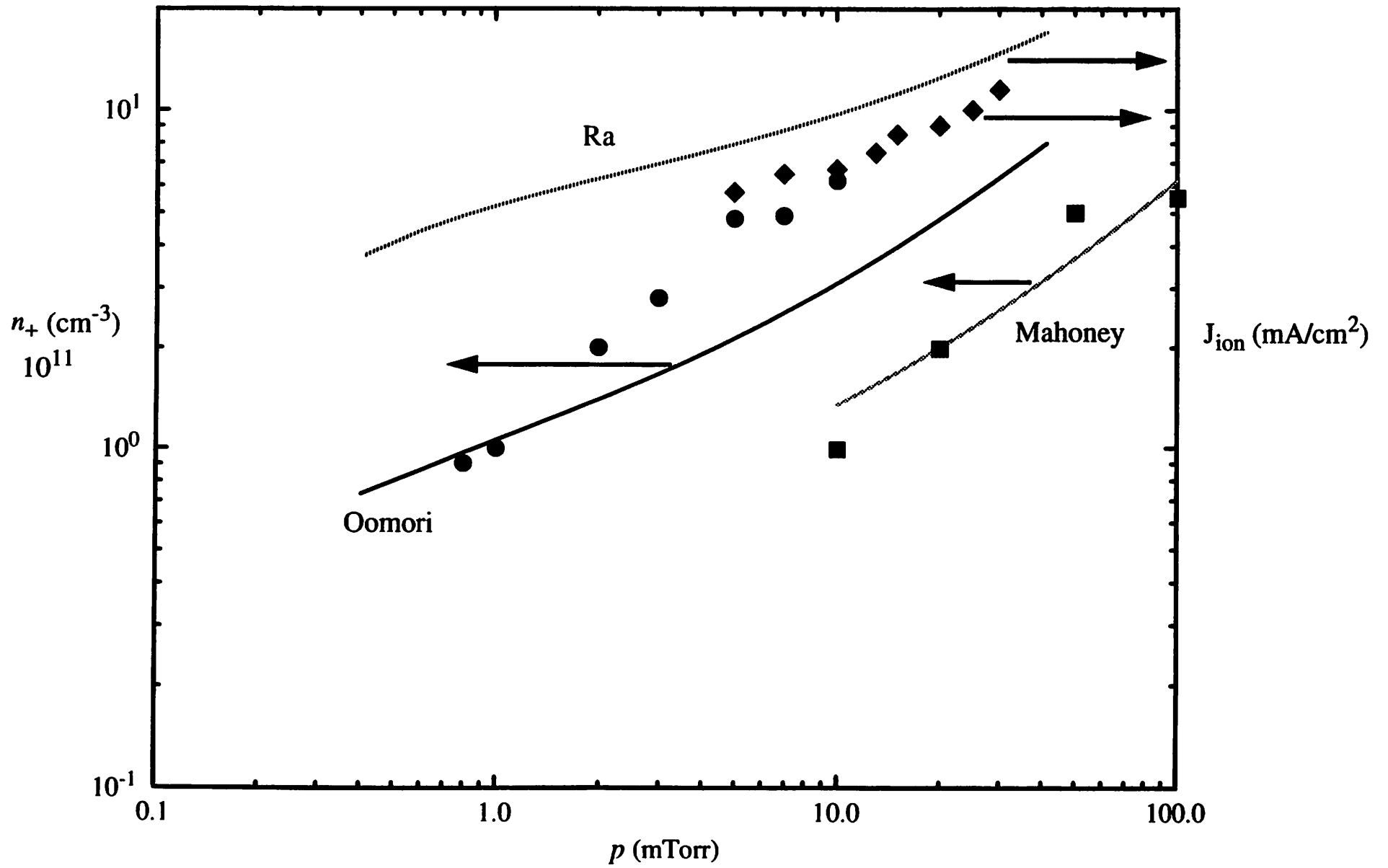


Figure 9.

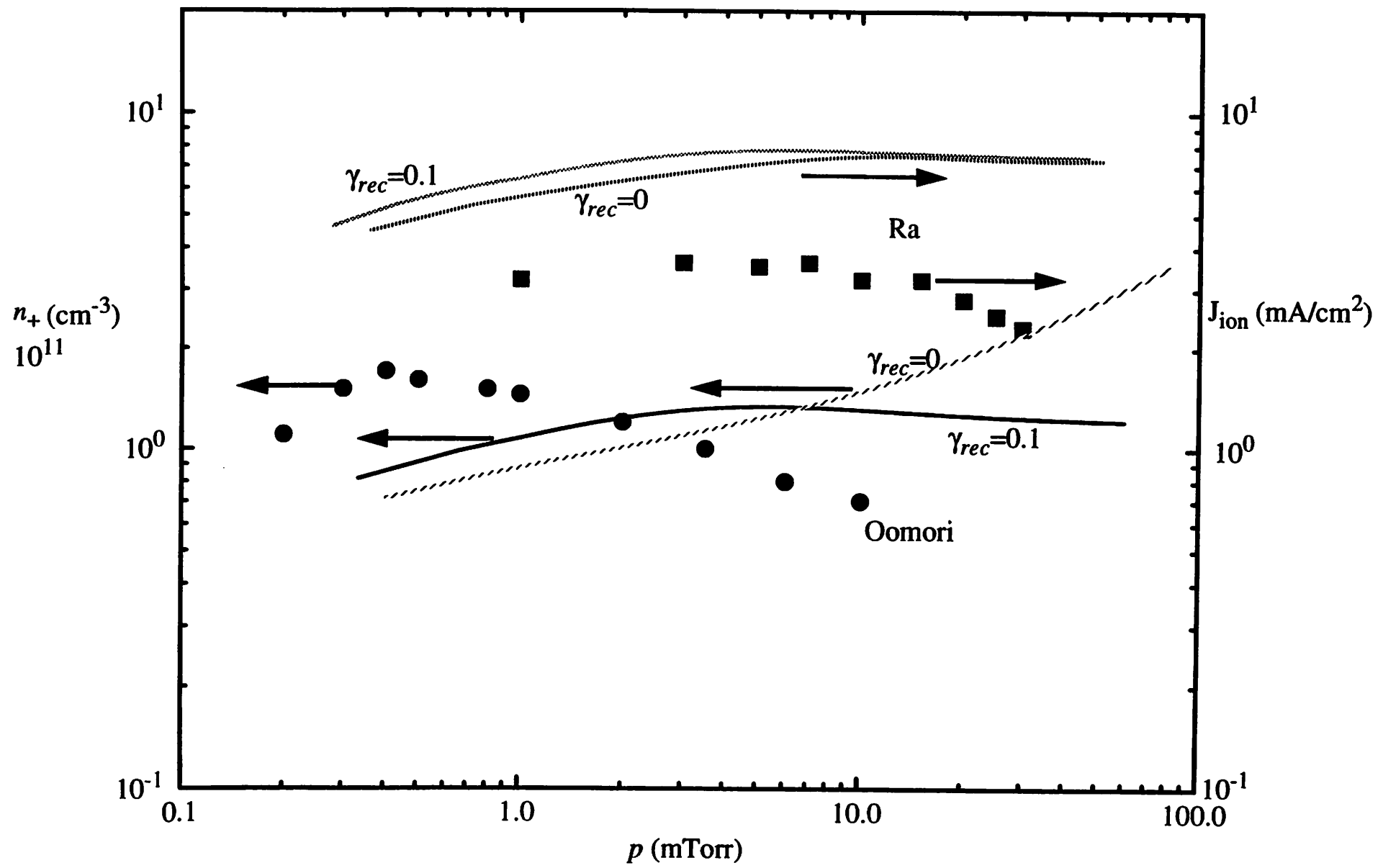


Fig 10

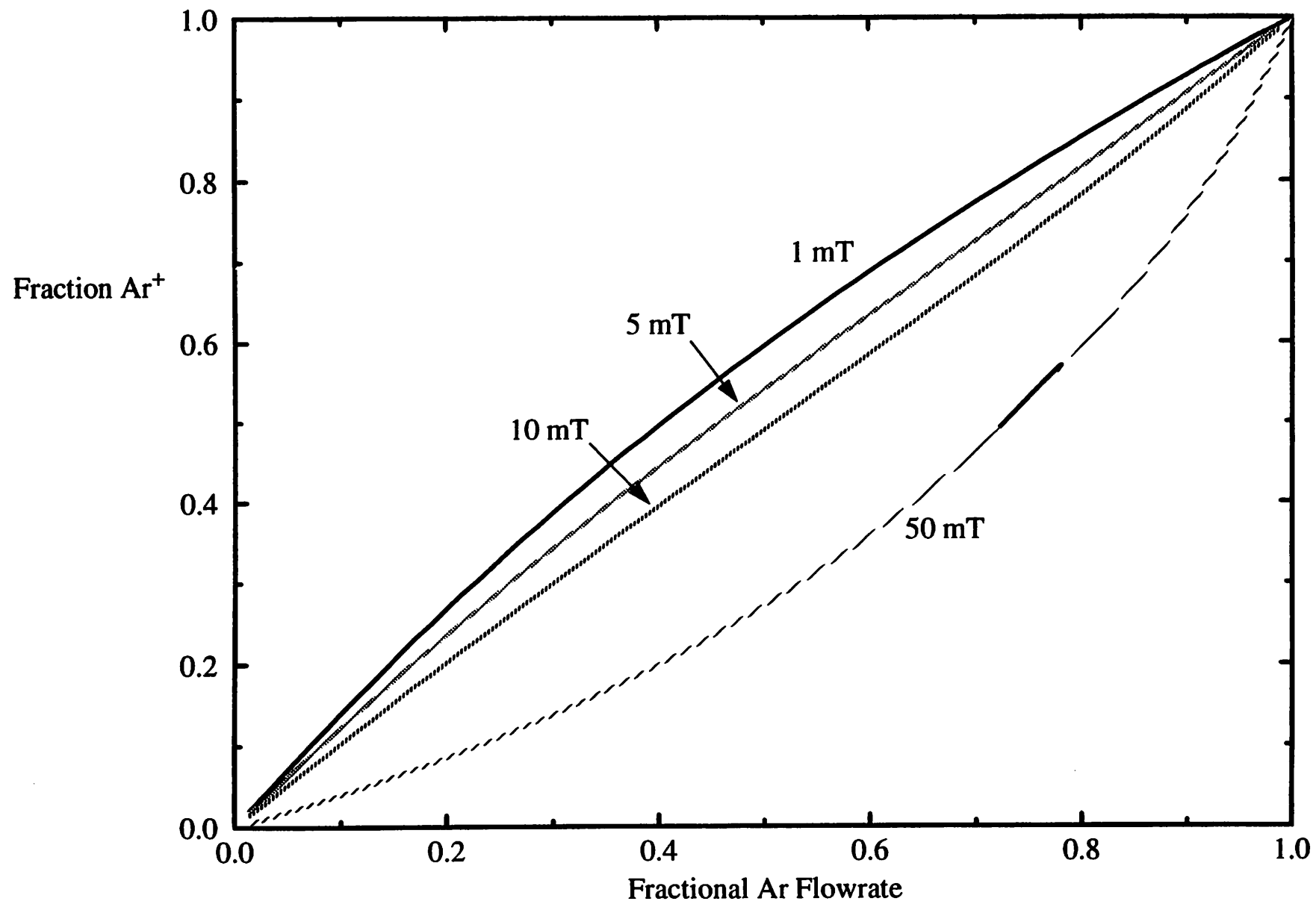


Fig 11

